130

LB63682

OF QUEENSLAND

DEPARTMENT OF CIVIL ENGINEERING

RESEARCH REPORT SERIES

Experiments on Smooth Cantilevered Circular Cylinders in Low-turbulence Uniform Flow

PART 1: Mean loading with Aspect Ratios in the range 4 to 30

T.A. FOX and G.S. WEST

**Research Report No. CE130
November 1991**

TA
1
.U4956
no. 130 etc.
Pt. 1

PSE

CIVIL ENGINEERING RESEARCH REPORTS

This report is one of a continuing series of Research
Reports published by the Department of Civil Engineering
at The University of Queensland. Lists of recently-
published titles of this series and of other publications
are provided inside the back cover of this report.
Requests for copies of any of these documents should be
addressed to the Departmental Secretary.

The interpretations and opinions expressed herein are
solely of the author(s). Considerable care has
been taken to ensure the accuracy of the material
presented. Nevertheless, responsibility for the use of
this material rests with the user.

EXPERIMENTS ON SMOOTH CANTILEVERED CIRCULAR CYLINDERS
IN A LOW-TURBULENCE UNIFORM FLOW
PART 1:MEAN LOADING WITH ASPECT RATIOS IN THE RANGE 4 TO 30

by

T.A.FOX, BSc(Surrey), PhD(Surrey)

Postdoctoral Research Fellow

and

G.S.WEST, BSc(Lond.), ME, PhD, MICE, MIMechE

RESEARCH REPORT No.CE130

Department of Civil Engineering

The University of Queensland

November 1991

SYNOPSIS

Part 1 of this report presents details of an investigation into the mean loading of smooth, cantilevered circular cylinders immersed in a low-turbulence uniform flow. Experiments were performed in a wind tunnel at a Reynolds number of 4.4×10^4 for aspect ratios in the range 4 to 30. Mean surface pressures and vortex shedding frequencies were measured, from which the local mean pressure drag and Strouhal number were calculated at various spanwise locations. The results reveal the extent of the disturbance induced by the flow around the free-end of a cantilever and the existence of a significant aspect ratio of 13.

CONTENTS

PSE
Exch.
3/92

1. INTRODUCTION

An understanding of the flow around a bluff body is often central to the solution of a wide range of engineering problems. This is particularly true of the circular cylinder, which is the bluff body shape most commonly encountered in industrial applications. Indeed, the fluid motion caused by the presence of a circular cylinder within a fluid stream induces both mean and fluctuating loads and, if the body is free to vibrate, oscillations which are of practical significance in areas as diverse as building aerodynamics and heat exchanger design.

The fundamental case of the flow around the centre section of an infinitely long circular cylinder immersed in a uniform stream has received the attention of numerous research workers in the past. Several recent reviews of published work in this area have been provided by Basu (1985), Basu (1986), Niemann and Hölscher (1990) and Zdravkovich (1990). However the flow around a cantilevered circular cylinder of finite-length immersed in a uniform stream, which is dominated by the presence of a free end and is therefore somewhat more complex, has received relatively little attention despite its considerable practical importance.

The free-end of a cantilevered circular cylinder induces strong three-dimensionality to the flow around the body and results in the formation of two intense longitudinal trailing vortices in the tip region, Gould et al. (1968), Okamoto and Yagita (1973) and Tyack (1989). These develop near the point of separation, a short distance from the free-end, and cause a considerable disturbance to the free shear layers in that region. At Reynolds numbers (based on cylinder diameter and freestream velocity) in the upper subcritical range,

Okamoto and Yagita (1973) and Farivar (1981) have found that the periodic vortex shedding process associated with the infinitely long circular cylinder is completely suppressed at the tip itself. If the cantilever is short, that is with an aspect ratio (length to diameter ratio) less than seven, $A < 7$, suppression extends to the root.

Okamoto and Yagita (1973) have examined in detail the effect of this disturbance upon the distribution of induced mean pressure drag on smooth, cantilevered circular cylinders immersed in a low-turbulence uniform flow. They found that over the range of aspect ratios considered: $1 \leq A \leq 12.5$, the additional vorticity introduced into the near wake at the free-end causes a large reduction in the wake pressures, resulting in high local mean pressure drag coefficients at positions near the tip. Indeed, the peak value of C_D was recorded at about half a diameter from the free-end in all cases. Further along the cylinder, they found that the effects of the longitudinal trailing vortex structure are much reduced and that the entrainment of fluid from the free-end relieves some of the negative pressure in the wake. Consequently the local peak in the tip region is followed by a steep reduction in C_D to values well below the infinite cylinder case on the major part of the cantilever (a similar result was recorded by Gould et al. (1968) at a transcritical Reynolds number).

In addition to mean parameters, some measurements of fluctuating surface pressures have been published by Farivar (1981) for cantilevers with aspect ratios less than 13. The results of this study, which was carried out at an upper subcritical Reynolds number, show that the maximum fluctuating pressure coefficients are less than those associated with the infinite cylinder at all locations on the cantilever. However, the spanwise distribution is non-uniform,

particularly when $A > 7$, and the variation is similar to that of mean pressures.   In this respect the intense vorticity introduced by flow over the free-end produces peak fluctuating pressures at about half a diameter from the tip, followed by a reduction towards the root of the model.

Accompanying the variation of surface pressure coefficients, both Okamoto and Yagita (1973) and Farivar (1981) have reported a reduction in the value of the vortex shedding frequency towards the free-end of the cantilevers examined in their studies.   The spanwise variation of Strouhal number based on velocity fluctuations in the wake measured by Okamoto and Yagita shows a gradual decrease with distance from the root, the reduction being most severe near the tip, whereas the Strouhal number based on surface pressure fluctuations recorded by Farivar reveals this reduction to be in the form of discrete steps. The latter result suggests a cellular structure to the vortex shedding in the near wake, similar to that found behind the infinitely long circular cylinder immersed in a shear flow, Griffin (1985) (in the infinite cylinder case the spanwise cells, each of a constant shedding frequency, form as a result of the interaction of the shear flow vorticity with the wake of the body). However, further detailed investigation is required to determine the nature of the cells that form at the rear of a cantilevered circular cylinder in uniform flow.

It is clear that despite the experimental effort invested by the authors cited above, published work on cantilevered circular cylinders is limited in scope and, in particular, concentrates on cases where the aspect ratio is less than 13.   No attempt has been made to determine the full extent of the free-end disturbance in terms of cylinder length.   The experimental work described in this report was therefore
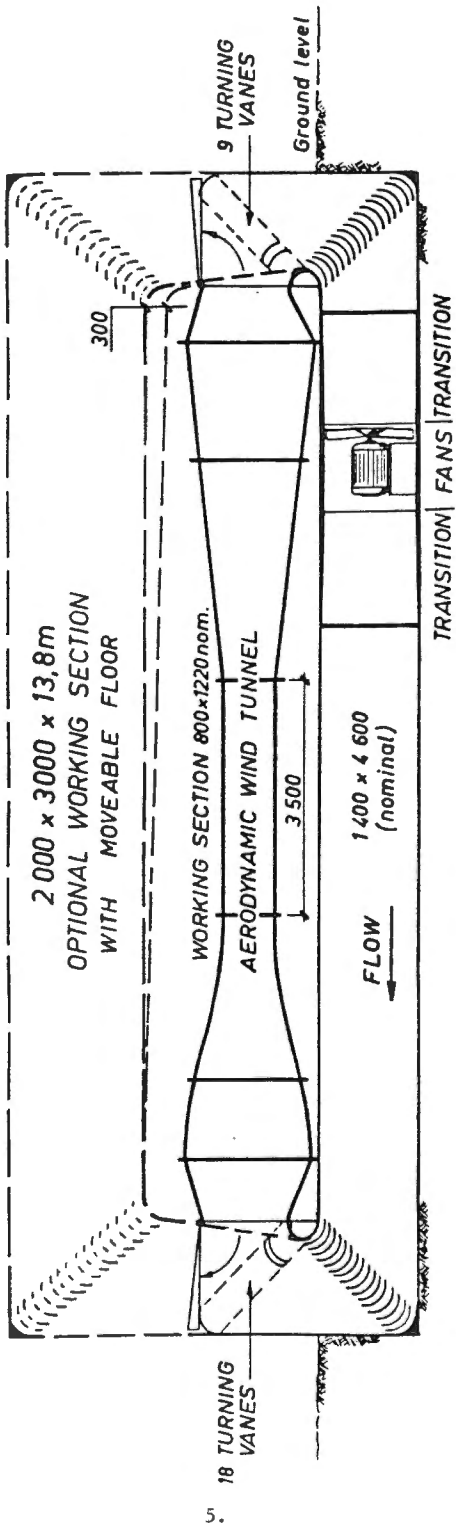
carried out to investigate the loading pattern on cantilevers with aspect ratios greater than 13 and to determine the characteristics of the disturbance induced by the free-end. To achieve this, measurements were made of mean surface pressure, mean pressure drag and vortex shedding frequency using smooth, cantilevered circular cylinders with aspect ratios in the range 4 to 30, as described here in Part 1, and of fluctuating pressure, rms lift and rms drag on a cantilever with an aspect ratio of 30, to be found in Part 2, Fox and West (1991), together with the results of a surface flow visualization study. Each cantilever was immersed in a low-turbulence uniform flow at a Reynolds number of Re $= 4.4 \times 10^4$ which, in the case of an infinitely long circular cylinder, is in the upper subcritical regime and therefore compatible with previous work in this field.

2. EXPERIMENTAL DETAILS

The experiments were carried out in the Department of Civil Engineering's low-speed closed circuit (No.3) wind tunnel facility which is illustrated schematically in Figure 1. This has an aerodynamic working section with nominal dimensions of 1.22m width x 0.8m height x 3.5m length and produces a steady uniform airflow with a freestream turbulence intensity of approximately 0.2% at the model testing position.

The cantilevered model used in the Part 1 experiments consisted of a long, smooth, polished, circular brass cylinder of 31.7mm diameter with a closed free-end. The cylinder entered the tunnel horizontally at mid-height, through a sealed hole in one of the side walls, and was fitted at the root with an aluminium end plate of the dimensions recommended by Stansby (1974). Figure 2 is a photograph of the

Figure 1: Schematic of the low-speed closed-circuit (No.3) wind tunnel facility.

(all dimensions in mm unless otherwise shown)

9 TURNING VANES

Ground level

300

2 000 × 3000 × 13,8m
OPTIONAL WORKING SECTION
WITH MOVEABLE FLOOR

WORKING SECTION 800×1220nom.

AERODYNAMIC WIND TUNNEL

3 500

FLOW

1400 × 4 600
(nominal)

TRANSITION | FANS | TRANSITION

18 TURNING VANES

5.
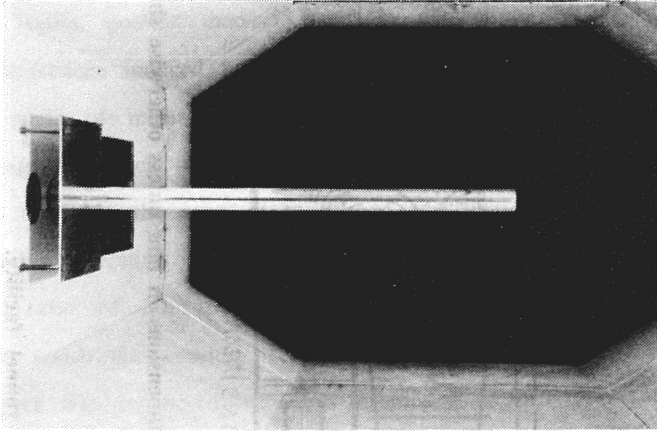
Figure 2: The model cantilever assembled in the working section prior to testing at an aspect ratio of 19.

complete assembly in the working section, prior to testing, at an aspect ratio of 19. Variations in the aspect ratio of the cantilever were achieved by sliding the model through the vertical wall. This arrangement permitted experiments on cantilevers with aspect ratios up to a maximum of 30, which was the largest possible without interference effects resulting from confinement of the flow between the free-end and the wind tunnel wall. The area blockage varied with the aspect ratio up to a maximum of 3.4% and it was therefore considered unnecessary to apply a correction to the data.

Mean pressures were measured on the surface of the model through a series of 1.0mm tappings arranged at intervals of one cylinder diameter along a single generator (the symmetry of the flow field was used for

initial alignment of each tapping). These were connected, in turn, to a Betz-type micromanometer, which could be read to within 0.1mm of water. A similar manometer was used across calibrated contraction tappings for the evaluation of the freestream reference pressure, from which the coefficient of mean pressure, Cp, was calculated using the relationship:

$$Cp = \frac{P - P_o}{\frac{1}{2}\rho U_o^2}$$

where P is mean local surface pressure, P_o is the freestream static pressure and $\frac{1}{2}\rho U_o^2$ is the dynamic pressure of the freestream. Circumferential pressure distributions were obtained by rotation of the cylinder.

The local mean pressure drag coefficient, C_D, was evaluated at various spanwise locations by numerical integration of the circumferential distribution of Cp in accordance with the expression:

$$C_D = \int_0^\pi Cp \cos\theta \, d\theta$$

where θ is the azimuth angle from the front stagnation point.

The frequency of vortex shedding from the cylinder was determined by analysis of the output signal from a constant temperature hot-wire anemometer mounted on a three-dimensional traversing system. The probe was of the DISA P11 type and was used unlinearized with a DISA 55M10 bridge unit. Signal analysis was performed on a B & K 2034 Signal

Analyzer, the frequency of shedding being determined from spectra, and the result is expressed as a Strouhal number:

$$St = \frac{nd}{U_o}$$

where n is the shedding frequency, d the cylinder diameter and U_o the freestream velocity.

3. RESULTS AND DISCUSSION

3.1 Mean Surface Pressure Distributions

The circumferential pressure distributions recorded at one diameter intervals along the length of cantilevers with aspect ratios in the range 4 to 30 are presented in Appendix III as Figures A1 to A10. From these Figures 3-12 have been constructed to show typical distributions at several spanwise locations (y/d as indicated on each plot), together with the corresponding curve for the infinitely long circular cylinder under the same test conditions. The latter was determined by extending the model across the full width of the tunnel and fitting a second end plate in accordance with the recommendations of Fox and West (1990). In each case the curves show that the entrainment of fluid into the wake by the downwash mechanism associated with flow over the free-end results in wake pressures that are generally higher than those associated with the infinite cylinder.

At the tip itself, the longitudinal trailing vortices generated in the wake of the cylinder cause a considerable distortion to the rear surface pressures. This disturbance is most clearly evident as a local minimum of pressure at around $\theta = 150^\circ$ in the distributions recorded at

Figure 4: Circumferential distributions of the mean pressure coefficient measured at y/d=1, 2, 4, 6 on the cantilevered circular cylinder with an aspect ratio of 7.
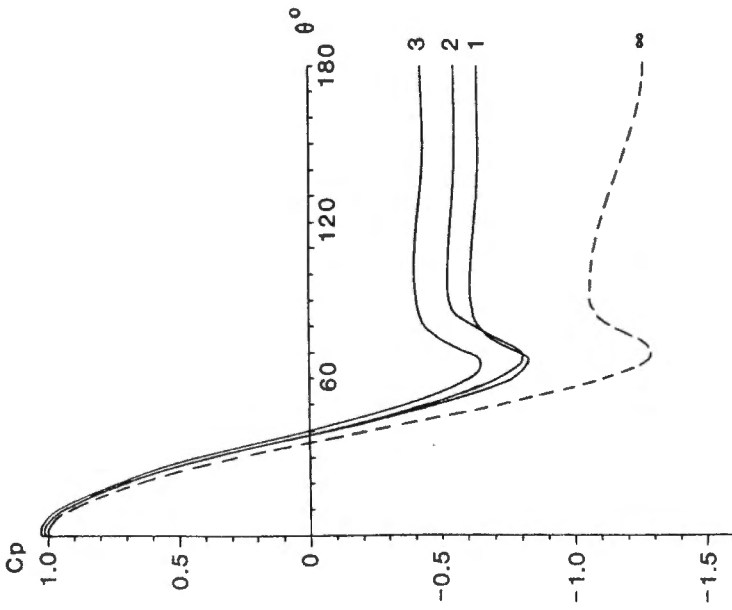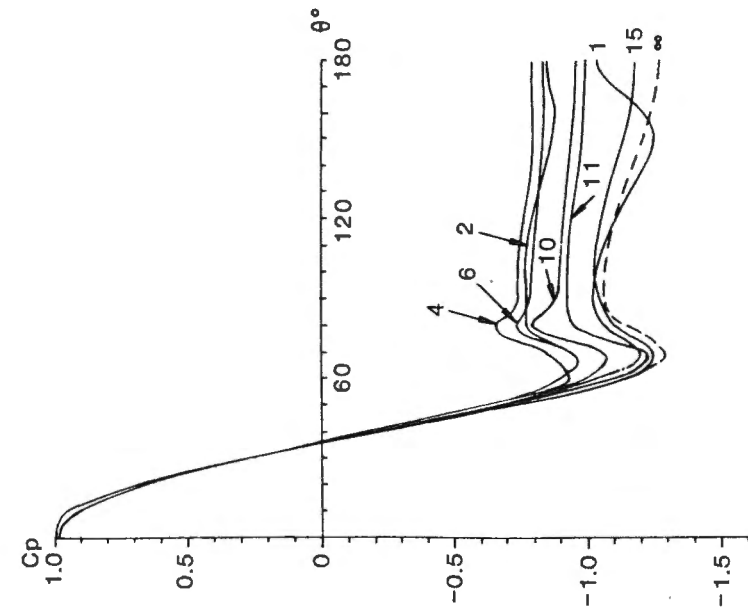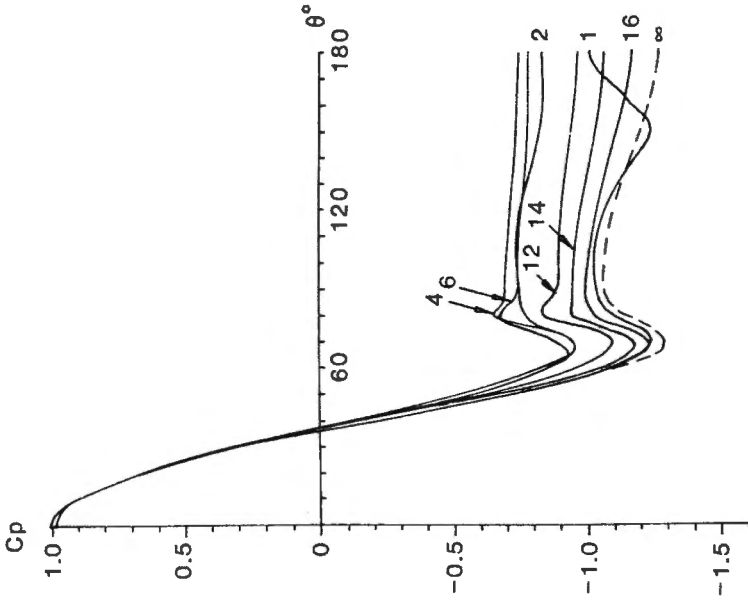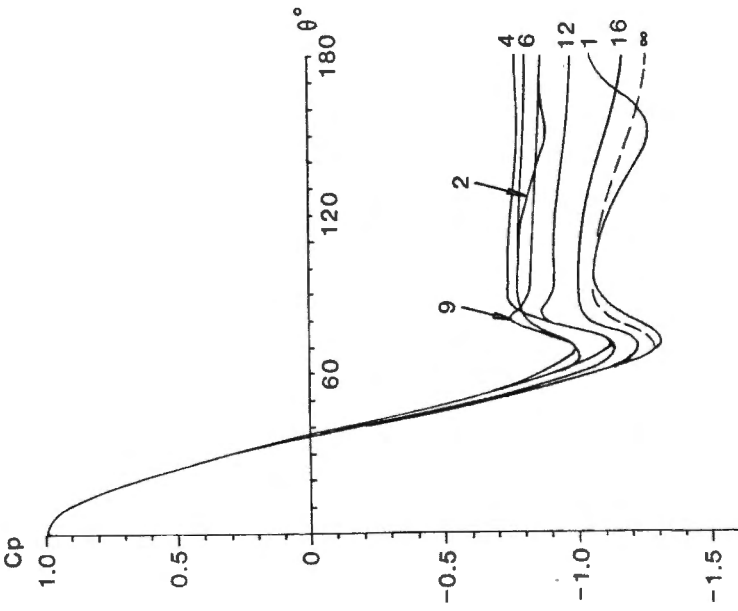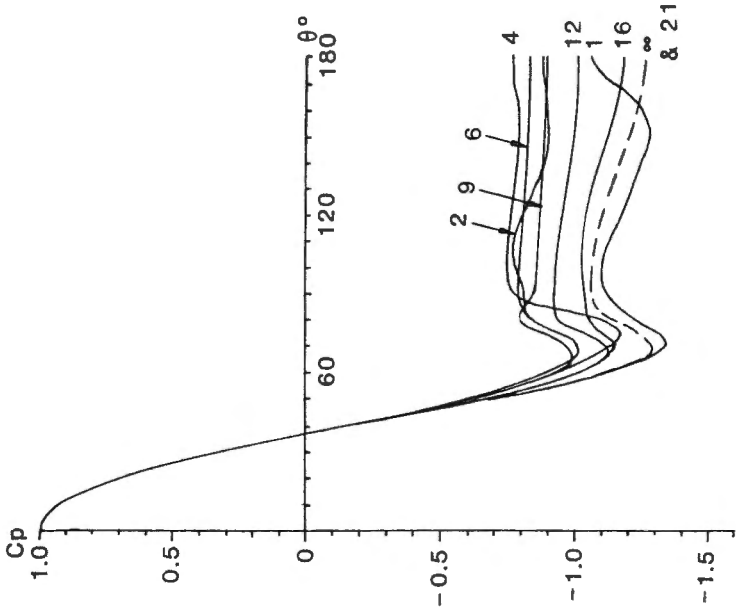

Figure 3: Circumferential distributions of the mean pressure coefficient measured at y/d=1, 2, 3 on the cantilevered circular cylinder with an aspect ratio of 4.
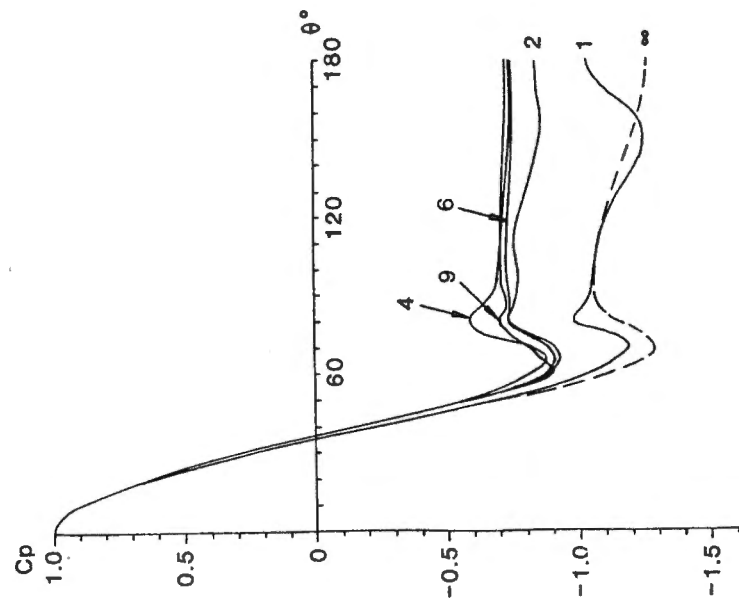
Figure 5: Circumferential distributions of the mean pressure coefficient measured at $y/d=1$, 2, 4, 6, 9 on the cantilevered circular cylinder with an aspect ratio of 10.
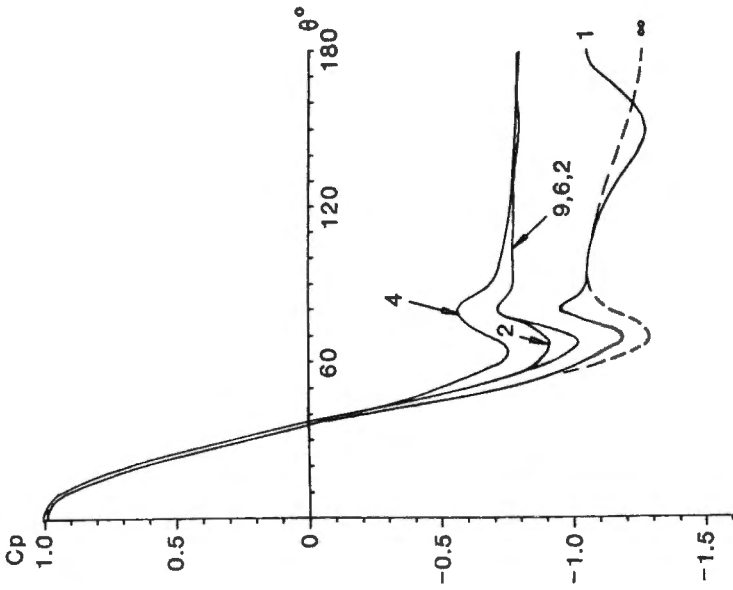
Figure 6: Circumferential distributions of the mean pressure coefficient measured at $y/d=1$, 2, 4, 6, 9 on the cantilevered circular cylinder with an aspect ratio of 11.
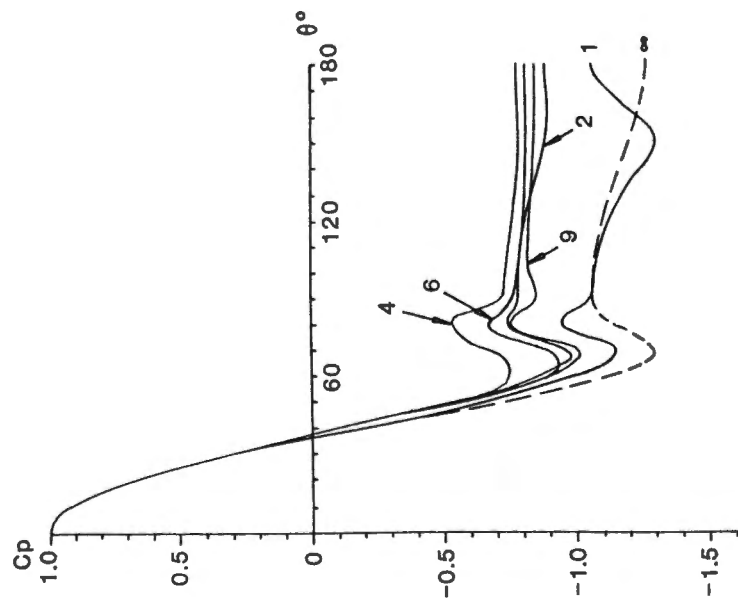
Figure 7: Circumferential distributions of the mean pressure coefficient measured at y/d=1, 2, 4, 6, 9 on the cantilevered circular cylinder with an aspect ratio of 12.
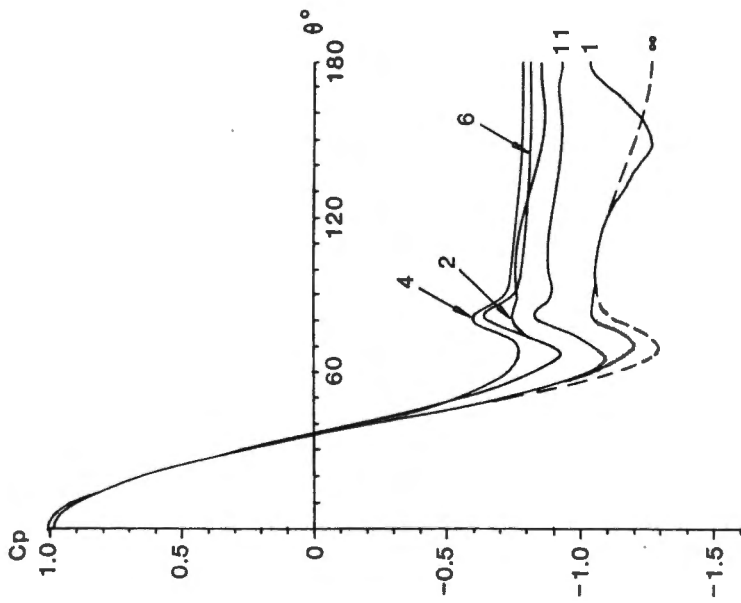
Figure 8: Circumferential distributions of the mean pressure coefficient measured at y/d=1, 2, 4, 6, 11 on the cantilevered circular cylinder with an aspect ratio of 13.

11.

Figure 9: Circumferential distributions of the mean pressure coefficient measured at y/d=1, 2, 4, 6, 10, 11, 15 on the cantilevered circular cylinder with an aspect ratio of 16.

Figure 10: Circumferential distributions of the mean pressure coefficient measured at y/d=1, 2, 4, 6, 12, 14, 16 on the cantilevered circular cylinder with an aspect ratio of 19.

Figure 11: Circumferential distributions of the mean pressure coefficient measured at y/d=1, 2, 4, 6, 9, 12, 16 on the cantilevered circular cylinder with an aspect ratio of 25.

Figure 12: Circumferential distributions of the mean pressure coefficient measured at y/d=1, 2, 4, 6, 9, 12, 16, 21 on the cantilevered circular cylinder with an aspect ratio of 30.

y/d=1 on all the cantilevers considered, except that with an aspect ratio of 4, Figure 3. In the latter case the post-separation pressures are constant at each spanwise location, which suggests that the longitudinal trailing vortices do not form in the wake of short cantilevers. Indeed, there is no evidence for the presence of such vortices in the results obtained by Uematsu et al. (1990) and Baban and So (1991) from experiments on cantilevers with aspect ratios in the range 1 to 4.

The longitudinal trailing vortices are evident as a weak feature in the $y/d=1$ profile recorded on the cantilever of aspect ratio $A=7$, Figure 4. In this case the distributions at locations away from the tip form a family of curves similar to that found in Figure 3, but with a minor disturbance evident near the separation point ($\theta \approx 80^{\circ}$). This is consistent with the results of Okamoto and Yagita (1973), who found that at an aspect ratio of 7 vortex shedding recommences at spanwise locations away from the tip, albeit somewhat disturbed shedding.

Figures 5-12 reveal that the wake pressures recorded at locations away from the tip on cantilevers with aspect ratios greater than seven can be divided into two distinct groups. In the first of these, that is when $7 < A \leq 13$, Figures 5-8, the downwash associated with flow over the free-end results in a significant distortion to the pressures around the separation point. This distortion is characterized by a distinct local maximum in the value of Cp at $\theta \approx 80^{\circ}$. In the second group, when $A > 13$, Figures 9-12, the distortion is also present, but is only significant at spanwise locations less than 11, 14, 16, and 12 diameters from the free-end of cantilevers with aspect ratios of 16, 19, 25, and 30 respectively. Beyond this the profiles return to the shape associated with the infinite cylinder.

Since Okamoto and Yagita (1973) have shown that for cantilevers with aspect ratios of seven or above vortex shedding is present at spanwise locations beyond the highly disturbed tip, the distortion described above is possibly related to an interference to the structure of the vortex formation region near the point of separation. This is considered further in Part 2, which presents the results of surface flow visualization experiments performed on a cantilever with an aspect ratio of 30.

The circumferential distributions presented in Figures 3-12 also show that the pressures recorded on the front face of each cantilever, $0° < \theta < 30°$, are generally invariant with spanwise location (y/d) and essentially the same as for the infinite cylinder. This is particularly evident in Figures 13-18, which have been constructed from Figures A1-A10 to illustrate the spanwise variation of surface pressure. These show the front face pressures to be constant along the major part of the cantilever, there being a slight decrease in the value of Cp in proximity to the tip when y/d < 3.

At azimuth angles greater than $30°$ the spanwise pressure distributions presented in Figures 13-18 exhibit characteristics which are dependent upon the length of the cantilever and thus the results can be divided into aspect ratio related groups. When A < 13, Figures 13 and 14, the distributions are similar to those found in the experiments performed by Okamoto and Yagita (1973). In this respect the shorter cantilevers, for which A ≤ 7, Figure 13 (a) and (b), present distributions which are unique to a given aspect ratio and are a result of the strong interference effects occurring along the full length of the model. In
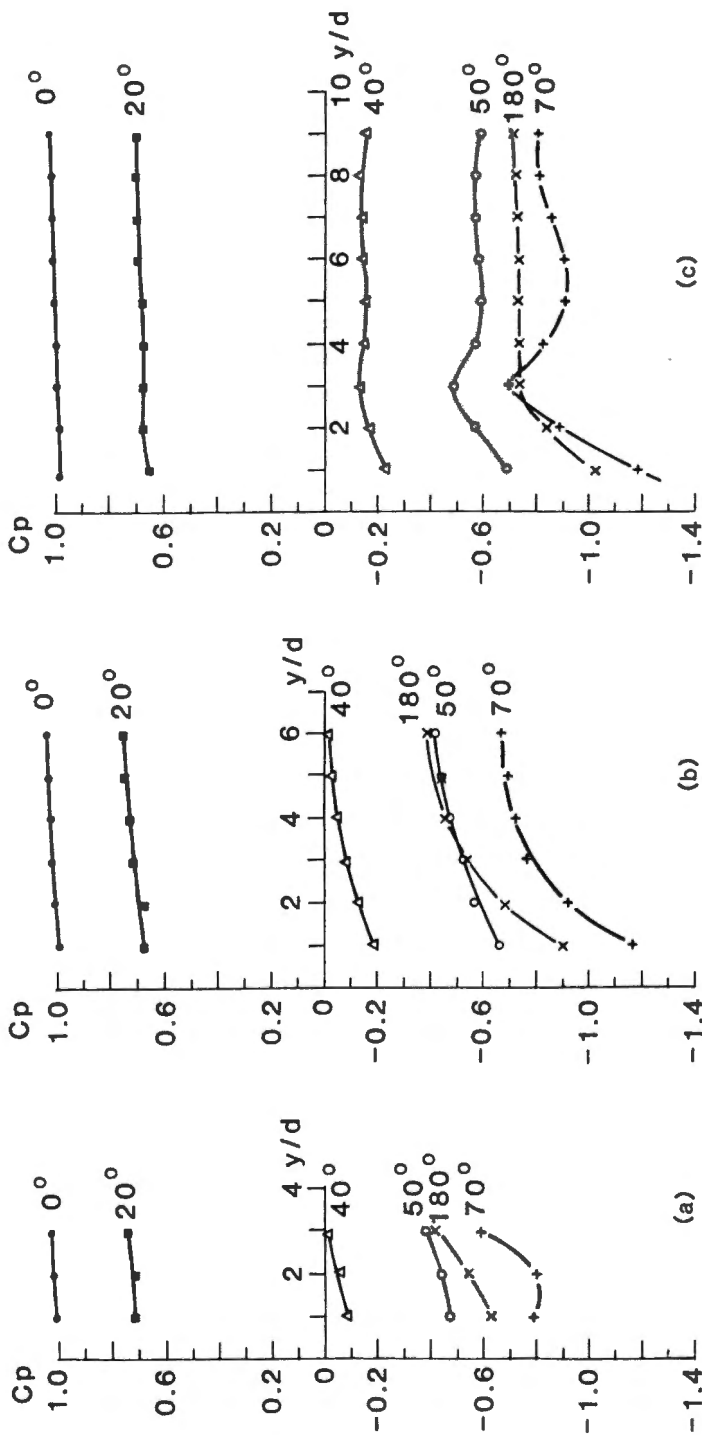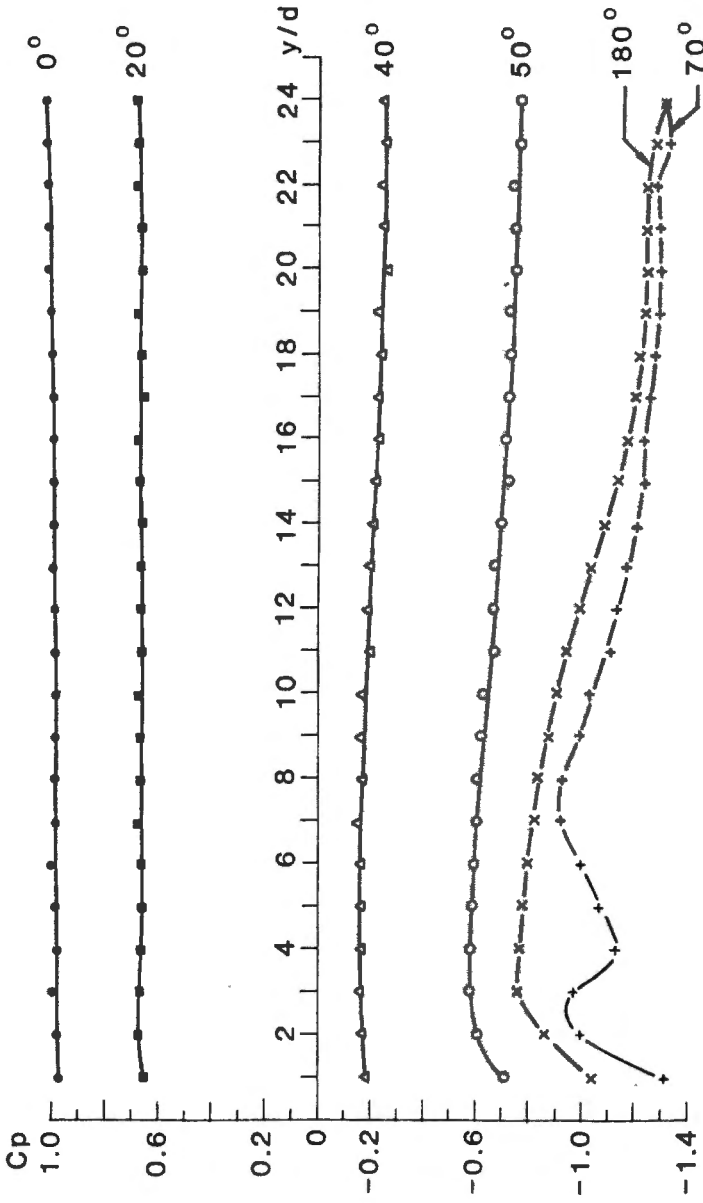
Figure 13: Spanwise distributions of the mean pressure coefficient measured at $\theta = 0^o$, 20°, 40°, 50°, 70°, 180° on cantilevered circular cylinders with aspect ratios of (a) 4, (b) 7, (c) 10.

16.
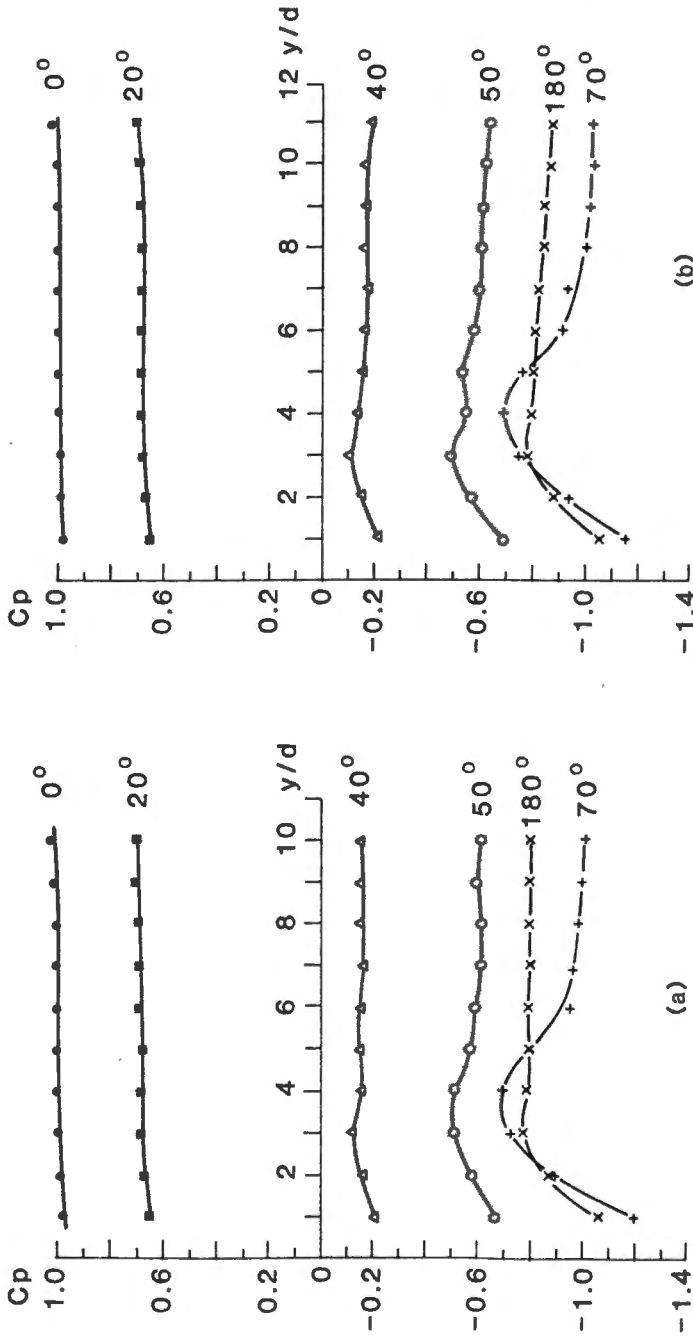
Figure 14: Spanwise distributions of the mean pressure coefficient measured at $\theta=0°$, $20°$, $40°$, $50°$, $70°$, $180°$ on cantilevered circular cylinders with aspect ratios of (a) 11, (b) 12.
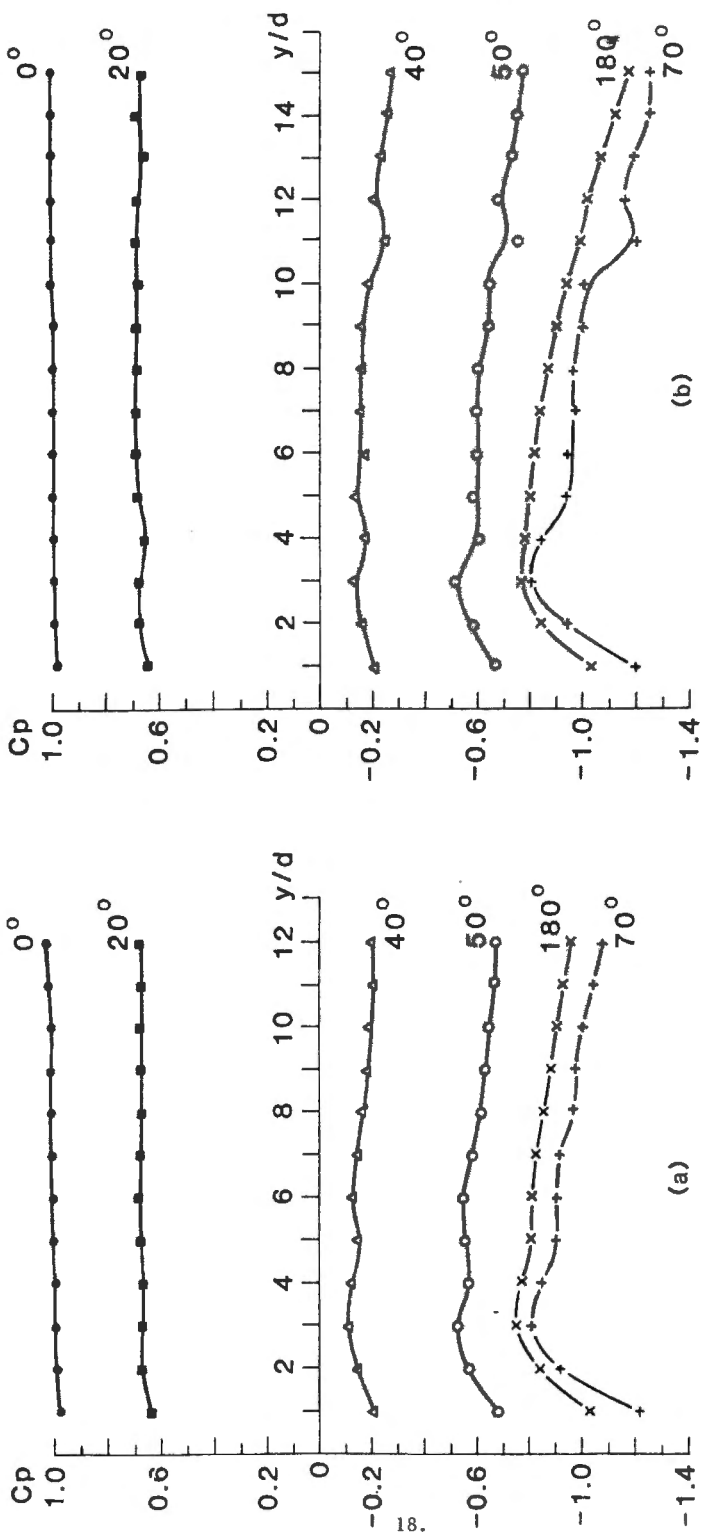
Figure 15: Spanwise distributions of the mean pressure coefficient measured at $\theta = 0°$, $20°$, $40°$, $50°$, $70°$, $180°$ on cantilevered circular cylinders with aspect ratios of (a) 13, (b) 16.

18.
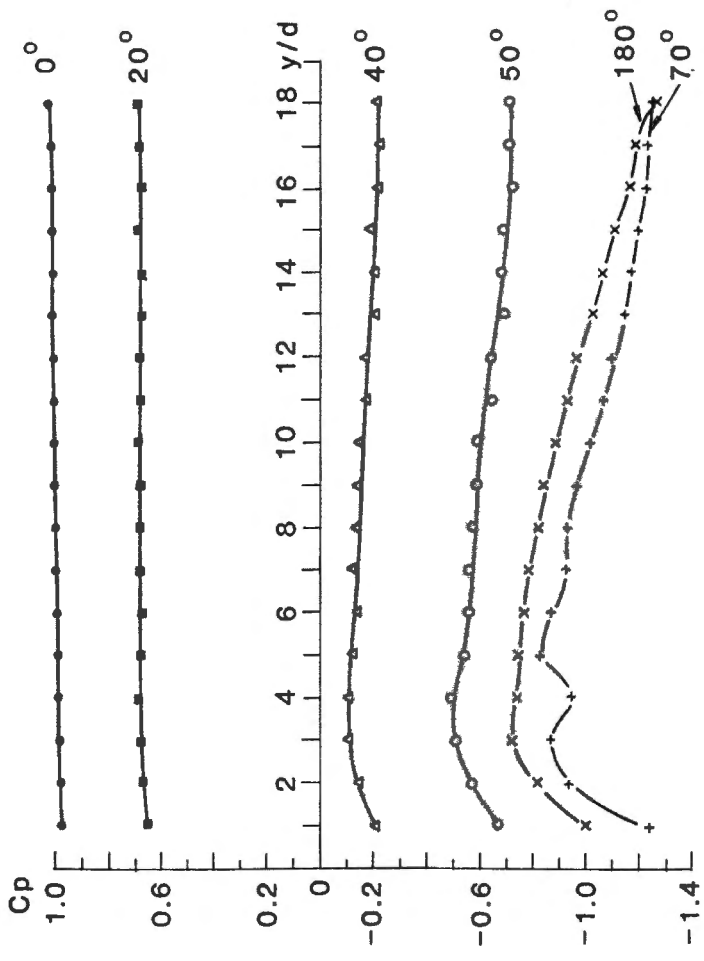
Figure 16: Spanwise distributions of the mean pressure coefficient measured at $\theta=0^o$, 20°, 40°, 50°, 70°, 180° on the cantilevered circular cylinder with an aspect ratio of 19.

19.

Figure 17: Spanwise distributions of the mean pressure coefficient measured at $\theta = 0°$, $20°$, $40°$, $50°$, $70°$, $180°$ on the cantilevered circular cylinder with an aspect ratio of 25.

20.
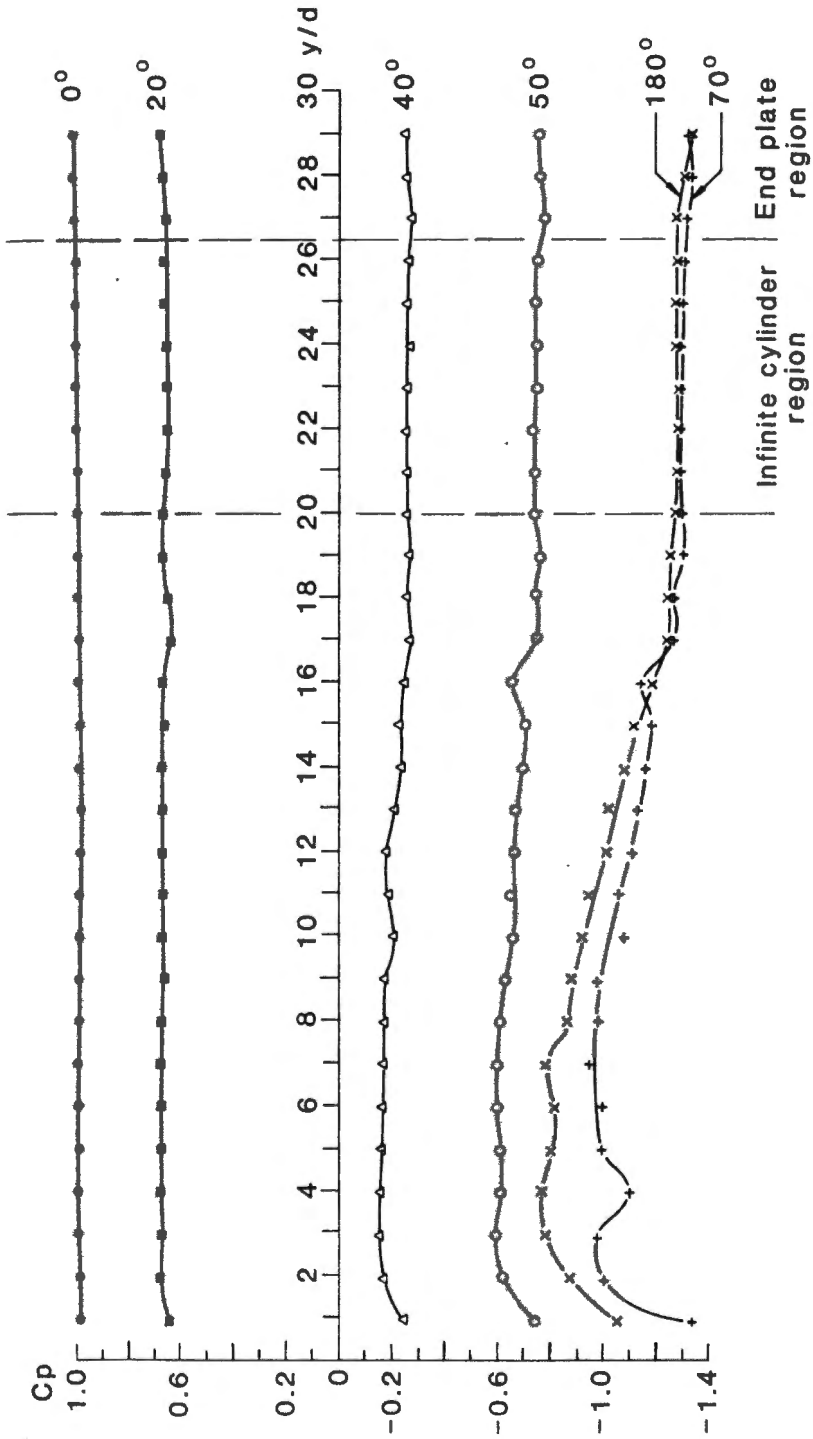
Figure 18: Spanwise distributions of the mean pressure coefficient measured at $\theta=0°$, $20°$, $40°$, $50°$, $70°$, $180°$ on the cantilevered circular cylinder with an aspect ratio of 30.

21.

the case of the longer cantilevers, those in Figures 13 (c) and 14 (a) and (b), which are essentially the same as each other, the three-dimensional disturbance caused by the longitudinal trailing vortices results in a minimum pressure at the tip followed by a rise to a local peak in the region $y/d = 3$ to 4. This peak is particularly strong in the pre-separation distribution recorded at $\theta = 70^\circ$, but is much reduced both in the wake, as evident on the base-line ($\theta = 180^\circ$), and towards the front face. The associated pressure gradient is indicative of a movement of fluid towards the trailing vortices at the tip, whereas on the root side of the peak, $y/d > 3$, the gradient is initially favourable towards the root, followed by a region of approximately constant pressure.

When the aspect ratio of the cantilever is 13, Figure 15 (a), the spanwise pressure distribution changes significantly. Although Cp still rises from a minimum at the tip to a peak at $y/d = 3$, the pressures no longer fall to a constant value in the region $y/d > 3$. Instead, the distributions exhibit a continuous reduction of pressure towards the root and are indicative of the presence of a considerable downwash region in the wake. This spanwise reduction is particularly evident in the case of cantilevers with aspect ratios of 16 and 19, Figure 15 (b) and Figure 16, for which it dominates the major part of the cylinder, and continues as far as $y/d = 20$ on models which are sufficiently long, as shown for example when $A = 25$ and $A = 30$, Figures 17 and 18. In the last case the full extent of the spanwise pressure distribution found on a cantilevered circular cylinder is evident with a region of infinite cylinder conditions, characterized by a constant value of Cp at each azimuth angle, following the end of the disturbed region at $y/d = 20$. This return to the flow conditions associated with an infinitely long circular cylinder is also evident in the undisturbed

circumferential pressure distributions recorded at y/d > 20, Figure 12 and Appendix II. Finally, Figure 18 shows that the surface pressures are disturbed within 3.5 diameters of the root of the cantilever because of interference effects associated with the end plate (as described previously by Fox and West (1990)).

3.2 Mean Pressure Drag

Integration of the numerous circumferential pressure distributions presented in Figures A1-A10 yields Figure 19 and 20 which show the spanwise variation of the local mean pressure drag coefficient, C_D for
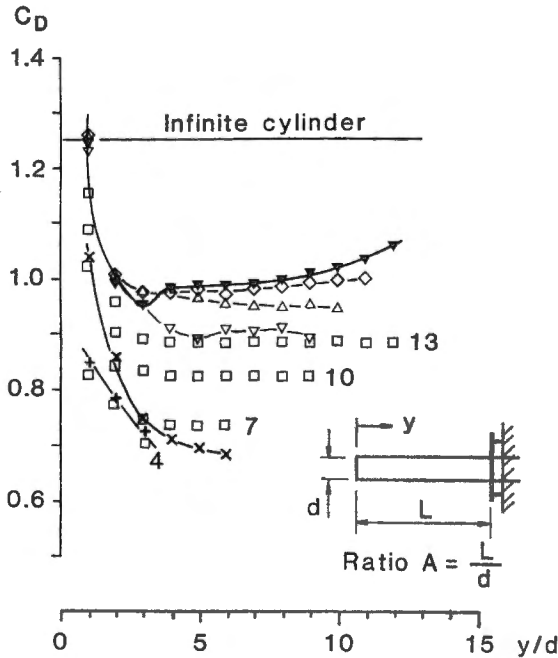
Figure 19: Spanwise distributions of the mean pressure drag coefficient on cantilevered circular cylinders with aspect ratios in the range A=4 to 13; + 4, × 7, ▽ 10, △ 11, ◇ 12, ▼ 13, □ E.S.D.U. 81017 (1981).

cantilevered cylinders with aspect ratios in the range 4 to 30, together with values calculated for selected cases using the design procedure given in E.S.D.U. 81017 (1981). The experimental results can be divided into two distinct groups depending on whether the aspect ratio is greater or less than 13, this being the significant aspect ratio identified in the surface pressure data. If A < 13, Figure 19, the distribution of drag along the cantilever is unique to a given aspect ratio, whereas for cases where A > 13, Figure 20, the values of C_D lie, with minor variations, on a single curve.

In the first of these two groups, when A < 13, Figure 19, the distribution of C_D is characterized by a rapid decrease in drag towards the root of the cantilever from a maximum near the free-end. If the cantilever is sufficiently long, as for example when the aspect ratio is 10, 11, and 12, the drag is approximately constant in the region y/d > 4, which is consistent with the findings of Okamoto and Yagita (1973). However, when A=13, C_D is no longer constant in this region, but instead shows a distinct rise towards the infinite cylinder value.

Figure 20 shows that the rise in C_D beyond $y/d = 4$ occurs on all cantilevers with aspect ratios greater than 13 and that the infinite cylinder value is, in fact, attained at $y/d=20$ on models of sufficient length. Indeed, the distribution of C_D presented in Figure 20 for A=30 shows the full extent of the drag variation found on a cantilevered cylinder, as further increases in the aspect ratio simply result in an extension of the region characterized by the infinite cylinder value. This ultimate distribution divides into four distinct regions. In the tip region adjacent to the free-end, y/d < 4 , the increased suction in the wake which results from the presence of the longitudinal trailing vortices induces a relatively high value of C_D. In this respect Figure

24.
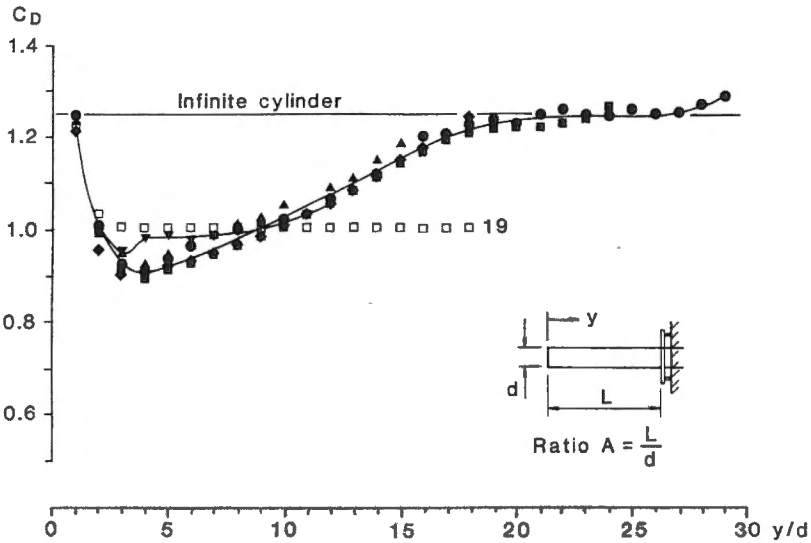
Figure 20: Spanwise distributions of the mean pressure drag coefficient on cantilevered circular cylinders with aspect ratios in the range A=13 to 30; ▼ 13, ▲ 16, ◆ 19, ■ 25, ● 30, □ E.S.D.U. 81017 (1981).

20 shows that at $y/d=1$ the local mean drag is of the order of that associated with the infinite cylinder. However, as y/d increases beyond 1, an increase in the wake pressures due to the entrainment of fluid over the free-end leads to a rapid decrease in C_D to a minimum value of 0.9 at $y/d=4$. The second region, $4 < y/d < 20$, is then characterized by a steady increase in C_D as the downwash in the wake is reduced with increased distance from the free-end. Eventually, by $y/d=20$, this interference effect no longer persists and the value of C_D reaches that associated with the undisturbed conditions of an infinitely long circular cylinder. Within this third region, the length of which is dependent upon the aspect ratio of the cantilever, C_D remains constant with spanwise position. The fourth region occurs

within 3.5 diameters of the root, where the interference effects of the end plate become significant, and is characterized by an increase in C_D as previously described by Fox and West (1990).

The experimental results presented in Figure 19 show good agreement with the drag coefficients calculated by the method of E.S.D.U. 81017 (1981) when A=4 and for y/d < 4 when A=7. There are, however, considerable differences at greater aspect ratios, as is particularly evident in Figure 20 for the A=19 case. It is suggested that this apparent discrepancy is due to the fact that E.S.D.U. 81017 (1981) is largely based on the results of Okamoto and Yagita (1973) and therefore assumes C_D to be constant for y/d > 4. Our results clearly show that this is not the case. However, it should be noted that the values of C_D close to the free-end are given correctly by E.S.D.U. 81017 (1981) for all aspect ratios considered.

3.3 Strouhal Number

The variation of the Strouhal number with spanwise location in the wake of each cantilever is presented in Figure 21 for models with aspect ratios in the range 10 to 30 (it was not possible to determine the vortex shedding frequency with confidence in the spectra recorded for aspect ratios less than 10). The results can be divided into the two distinct aspect ratio related groups previously defined by the mean pressure data. If A < 13, the Strouhal number variation is unique to the given aspect ratio, whereas for cases where A ≥ 13 the value of St at any given spanwise location is independent of aspect ratio.

When the aspect ratio is less than 13, the Strouhal number rises from a minimum near the free-end to a constant value in the region y/d > 6 and
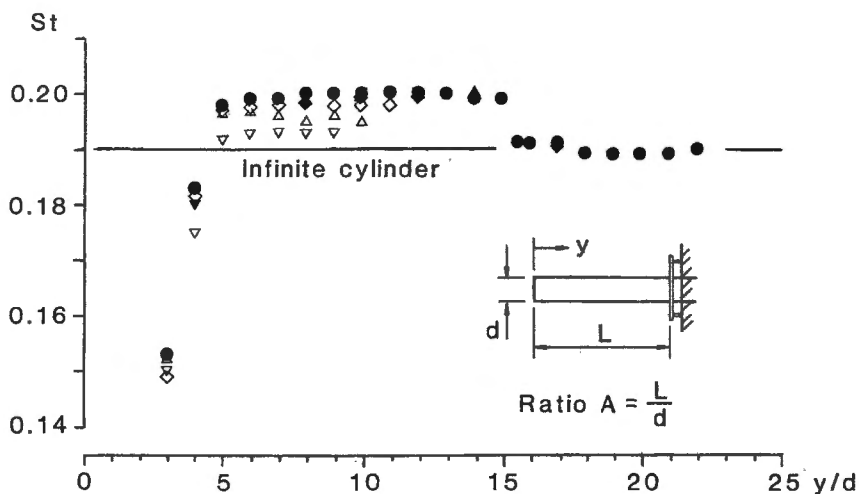
Figure 21: Strouhal number variation in the wake of cantilevered circular cylinders with aspect ratios in the range A=10 to 30; ▽ 10 △ 11, ◇ 12, ▼ 13, ▲ 16, ◆ 19, ■ 25, ● 30.

is, in this respect, similar to that previously found by Okamoto and Yagita (1973) in the wake of cantilevers of A=9 and A=12. However in Okamoto and Yagita's case the constant value was found to be considerably below that recorded in the wake of the infinite cylinder, whereas in our study it is equivalent to, or greater than, that value. At the tip itself it was not possible to detect a shedding frequency in the spectra. Indeed, Tyack (1989) has shown that in this region the free shear layer is prevented from rolling-up by the three-dimensional disturbance in the wake.

Figure 22 presents the spectrum recorded in the wake of the cantilever of aspect ratio A=12 at spanwise location y/d=4. The result is typical of spectra found in the region y/d < 6 on all of the cantilevers
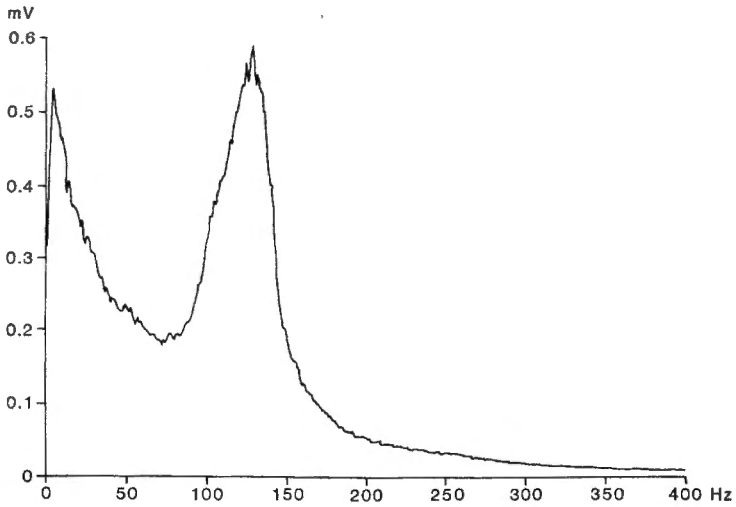
Figure 22: Spectrum of the velocity fluctuations at y/d=4 in the wake of a cantilevered circular cylinder with an aspect ratio of 12. Wire position: x=z=2d.
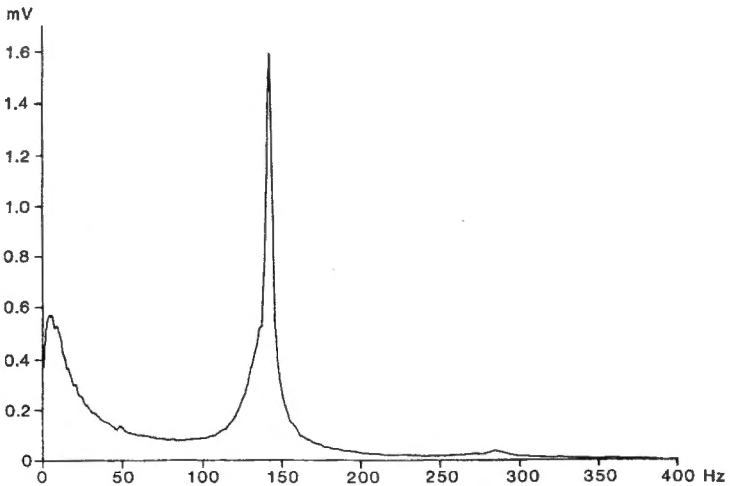
Figure 23: Spectrum of the velocity fluctuations at y/d=8 in the wake of a cantilevered circular cylinder with an aspect ratio of 12. Wire position: x=z=2d.

examined. These exhibit a wide spread of energy with an ill-defined dominant frequency and reflect the highly disturbed nature of vortex shedding in proximity to the tip. In contrast, the spectra recorded in the region y/d > 6 display a single well defined peak at a Strouhal frequency greater than that associated with the infinite cylinder, as evident in Figure 23 which shows the result in the wake of the same model at y/d=8. The value of this Strouhal frequency increases with aspect ratio until reaching a maximum at A = 13 and is indicative of the dominance of vortex shedding upon the fluid motion in this second region.

In the case of cantilevers with aspect ratios of 13 and above, Figure 21 shows that the variation of Strouhal number with spanwise location is fixed regardless of aspect ratio. Further, if the cantilever is sufficiently long, for example when A=19, 25 or 30, the high value of St is recorded in the wake up to y/d=15, where a discontinuity occurs with a return of the Strouhal number to the infinite cylinder value. The nature of this discontinuity is evident in Figure 24 which presents the spectra recorded at y/d=14.5, 15, 15.5, and 18 in the wake of the A=30 model. At y/d=14.5 a second, smaller, peak appears in the spectrum in addition to that associated with the dominant frequency. This second peak is at the infinite cylinder frequency, which is below the dominant frequency in the fluid motion. By y/d=15 the two peaks in the spectrum are of approximately the same magnitude. At y/d=15.5 the infinite cylinder peak clearly dominates and, therefore, the frequency change is complete. Indeed, the spectra recorded at all spanwise locations with increased distance from the discontinuity, at y/d=18 for example, display a single, well defined peak at the infinite cylinder frequency.
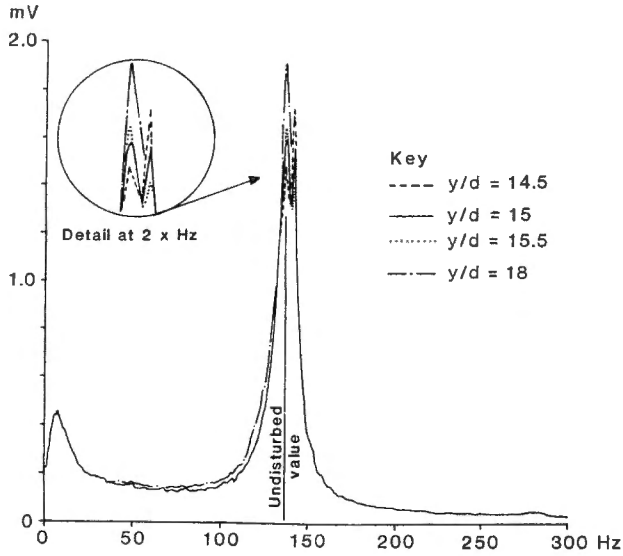
Figure 24: Spectra of the velocity fluctuations at y/d=14.5, 15, 15.5, and 18 in the wake of a cantilevered circular cylinder with an aspect ratio of 30.   Wire position: x=z=2d.

To satisfy the boundary conditions of these two distinct vortex shedding regions it is postulated that some form of longitudinal vortex mechanism exists at the frequency discontinuity.   This postulation is based upon the work of Maull and Young (1973), who found that a similar discontinuity with two frequency peaks could be obtained in the wake of a D-section body in uniform flow when a longitudinal trailing vortex was generated on its surface.

Apart from the discontinuity at y/d=15, in all of the cases considered in the current study there is no evidence for the existence of a cellular structure to the vortex shedding from the cantilever in the Strouhal number variation recorded with a hot-wire anemometer. This result is consistent with previous work, as reported by Basu (1986),

which has shown that Strouhal measurements based on velocity fluctuations in the wake tend to mask the discrete steps associated with the presence of such a structure. This phenomenon will therefore be considered in detail in Part 2, which presents Strouhal numbers based on pressure fluctuations at the surface of the model.

4. CONCLUSIONS

The experiments described in Part 1 of this report have provided details of the mean loading on smooth, cantilevered circular cylinders with aspect ratios of 4 to 30 immersed in a low-turbulence, uniform flow at a Reynolds number of 4.4×10^4 . It was found that:

(i)   there exists a significant aspect ratio of 13 with regard to the mean pressure distributions, the mean pressure drag and the spanwise variation of Strouhal number. If $A < 13$, the results are unique to a given aspect ratio, whereas if $A > 13$ the values at a given location are independent of aspect ratio.

(ii)   in general, the effect of the flow over the free-end is to increase the wake pressures, relative to that associated with the infinitely long circular cylinder, and therefore reduce the pressure drag on the major part of the cantilever.

(iii)   if the cantilever is sufficiently long, the interference to mean loading persists to a distance of 20 cylinder diameters from the free-end, beyond which conditions associated with the infinitely long circular cylinder are established.

31.

(iv)   the Strouhal number of vortex shedding from the cantilever is affected to a distance of 15 diameters from the tip, where a distinct discontinuity occurs dividing a region of relatively high Strouhal number from one of infinite cylinder value.

(v)   the procedures recommended in E.S.D.U. 81017 (1981) are not appropriate for the design of cantilevers with aspect ratios greater than 13 as they do not account for the return to infinite cylinder conditions.

5. ACKNOWLEDGEMENTS

APPENDIX I : REFERENCES

Baban, F.; So, R.M.C. 1991: Recirculating flow behind and unsteady forces on finite-span circular cylinders in a cross-flow. Journal of Fluids and Structures 5, 185-206.

Basu, R.I. 1985: Aerodynamic forces on structures of circular cross-section. Part 1. Model-scale data obtained under two-dimensional conditions in low-turbulence streams. Journal of Wind Eng. & Ind. Aerodyn. 21, 273-294.

Basu, R.I. 1986: Aerodynamic forces on structures of circular cross-section. Part 2. The influence of turbulence and three-dimensional effects. Journal of Wind Eng. & Ind. Aerodyn. 24, 33-59.

E.S.D.U. Item No 81017 1981: Mean forces, pressures and moments for circular cylindrical structures: finite-length cylinders in uniform and shear flow. Engineering Sciences Data Unit, London.

Farivar, Dj. 1981: Turbulent uniform flow around cylinders of finite length. AIAA Journal 19, 275-281.

Fox, T.A.; West, G.S. 1990: On the use of end plates with circular cylinders. Experiments in Fluids 9, 237-239.

Fox, T.A.; West, G.S. 1991: Experiments on smooth cantilevered circular cylinders in a low-turbulence uniform flow. Part 2: fluctuating loads on a cantilever of aspect ratio 30. Research Report No.CE131, Dept. Civil Eng., The University of Queensland.

Gould, R.W.E.; Raymer, W.G.; Ponsford, P.J. 1968: Wind tunnel tests on chimneys of circular section at high Reynolds numbers. Proc. Symp. on Wind Effects on Buildings and Structures, Loughborough University of Technology, Loughborough, England.

Griffin, O.M. 1985: Vortex shedding from bluff bodies in a shear flow: a review. ASME Journal of Fluids Engineering 107, 298-306.

Maull, D.J.; Young, R.A. 1973: Vortex shedding from bluff bodies in a shear flow. Journal of Fluid Mechanics 60, 401-409.

Niemann, H.-J.; Hölscher, N. 1990: A review of recent experiments on the flow past circular cylinders. Journal of Wind Eng. & Ind. Aerodyn. 33, 197-209.

Okamoto, T.; Yagita, M. 1973: The experimental investigation on the flow past a circular cylinder of finite length placed normal to the plane surface in a uniform stream. Bull. Japan Soc. Mech. Engrs 16, 805-814.

Stansby, P.K. 1974: The effects of end plates on the base pressure coefficient of a circular cylinder. Aeronaut. Journal 78, 36-37.

Tyack, M. 1989: Development of visualisation techniques and their application in investigating flow around a cylinder of finite length. B.Eng. Thesis, The University of Queensland.

Uematsu, Y.; Yamada, M; Ishii, K. 1990: Some effects of free-stream turbulence on the flow past a cantilevered circular cylinder. Journal of Wind Eng. & Ind. Aerodyn. 33, 43-52.

Zdravkovich, M.M. 1990: Conceptual overview of laminar and turbulent flows past smooth and rough circular cylinders. Journal of Wind Eng. & Ind. Aerodyn. 33, 53-62.

APPENDIX II : NOTATION

A   aspect ratio $= \dfrac{L}{d}$

C_D coefficient of mean pressure drag $= \int_0^\pi Cp \cos\theta \; d\theta$

Cp   coefficient of mean pressure $= \dfrac{P-P_0}{\frac{1}{2}\rho U_0^2}$

d   cylinder diameter

L   cantilever length

n   shedding frequency

P   mean local surface pressure

P_0 static pressure

Re   Reynolds number $= \dfrac{dU_0}{\upsilon}$

St   Strouhal number $= \dfrac{nd}{U_0}$

U_0 freestream velocity

y   distance from free-end

θ azimuth angle from stagnation point

υ kinematic viscosity of air

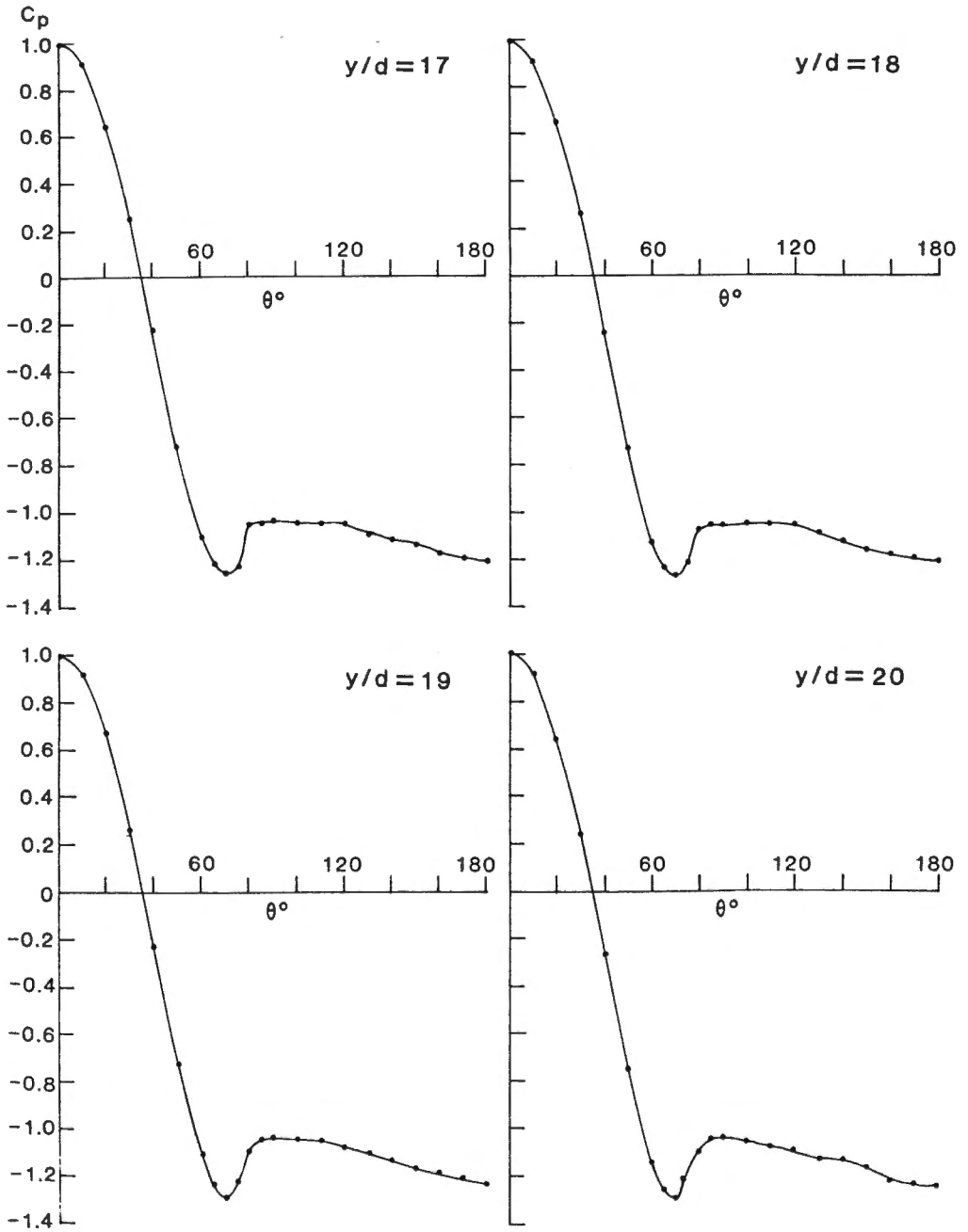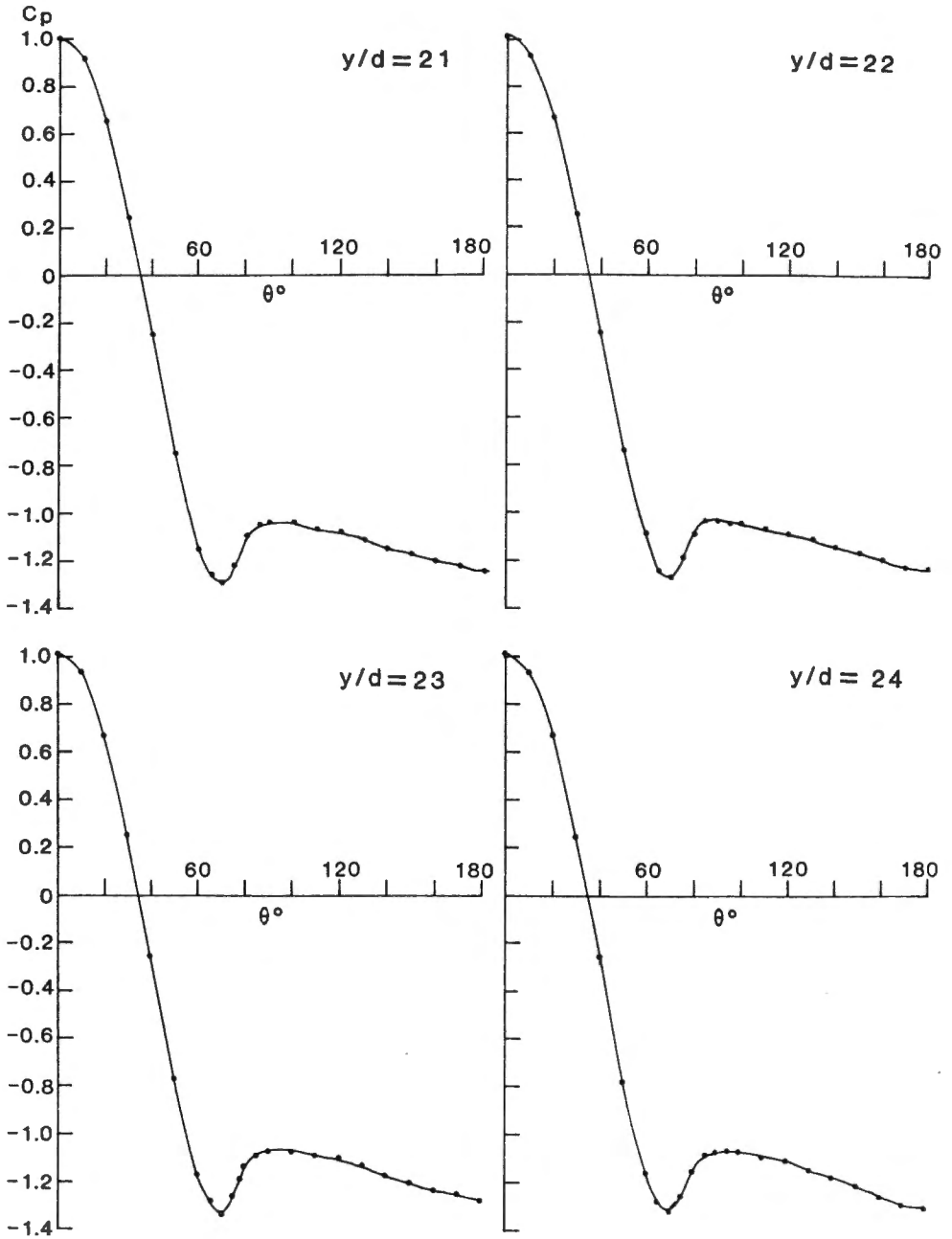ρ density of air

APPENDIX III : FIGURES A1-A10
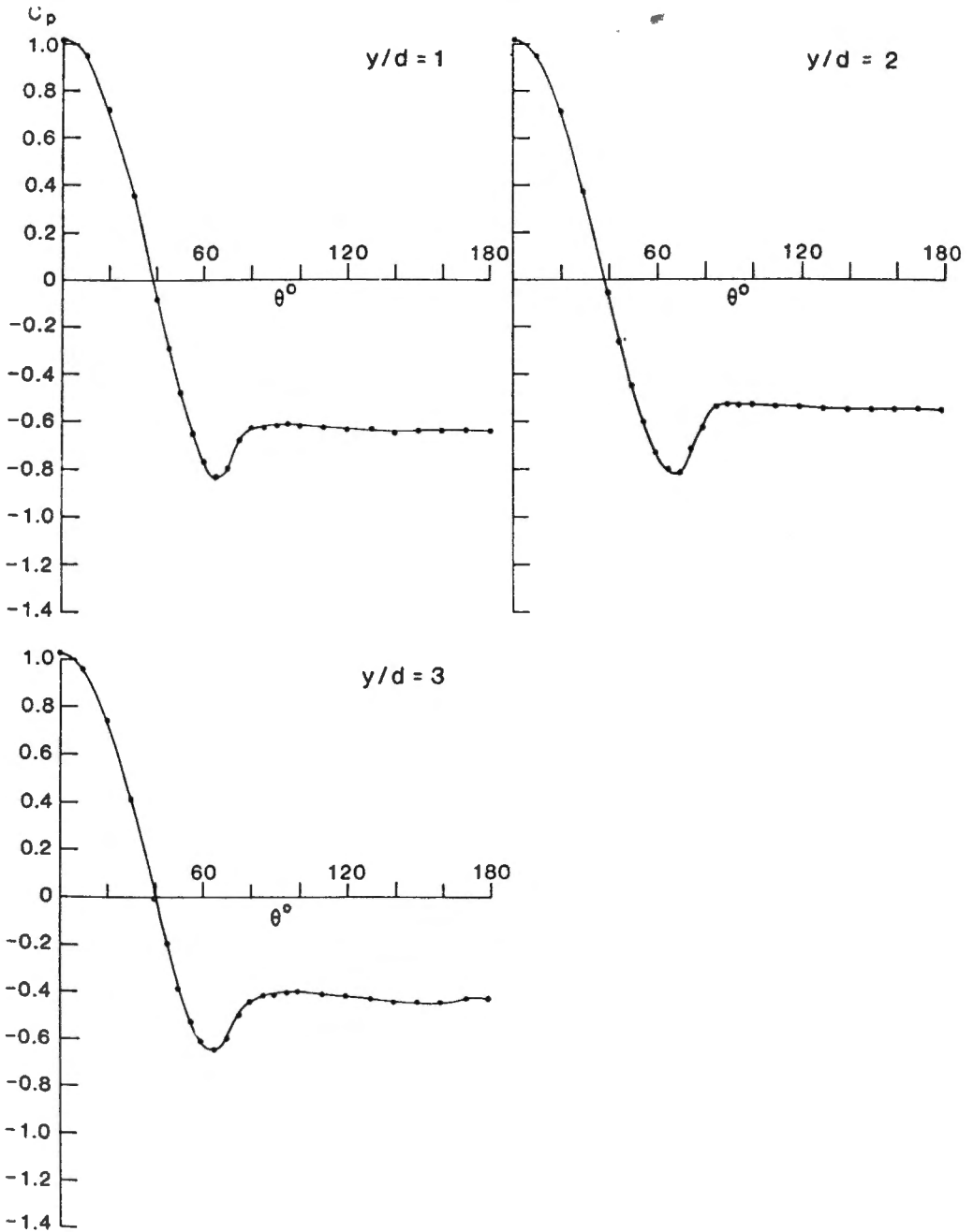
Figure A1: Circumferential distributions of the mean pressure coefficient measured on the cantilevered circular cylinder with an aspect ratio of 4.
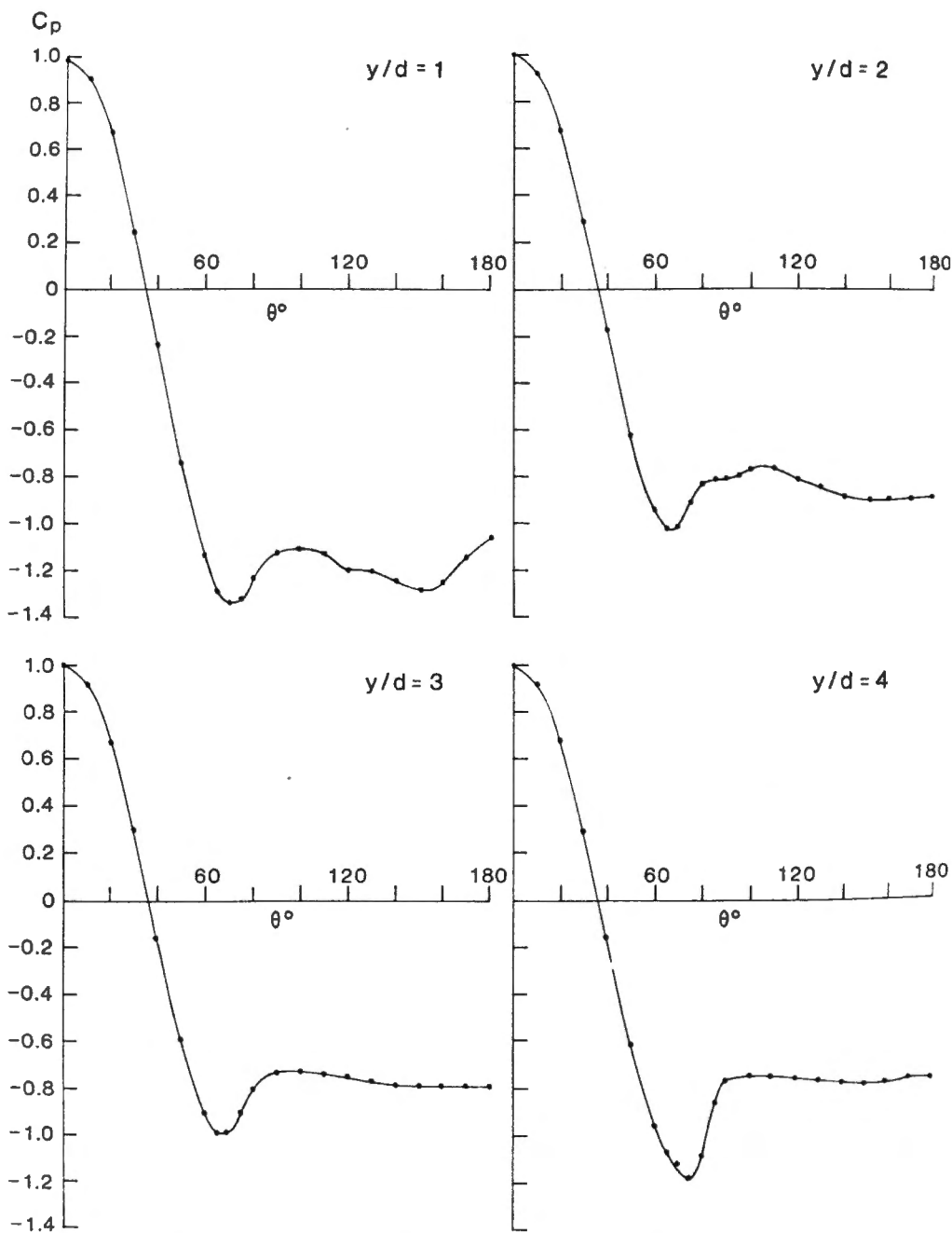
38.
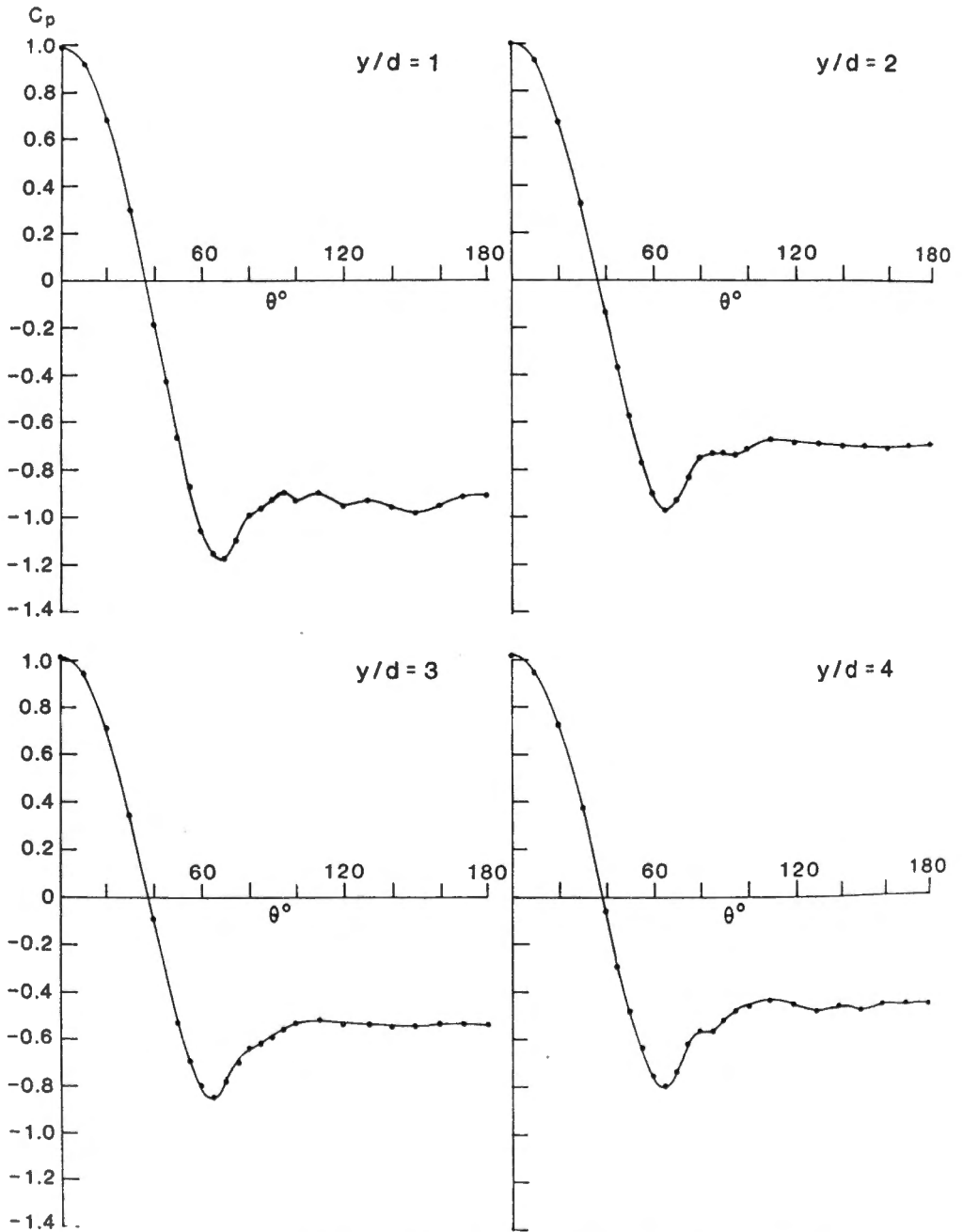
**Figure A2:** Circumferential distributions of the mean pressure coefficient measured on the cantilevered circular cylinder with an aspect ratio of 7.
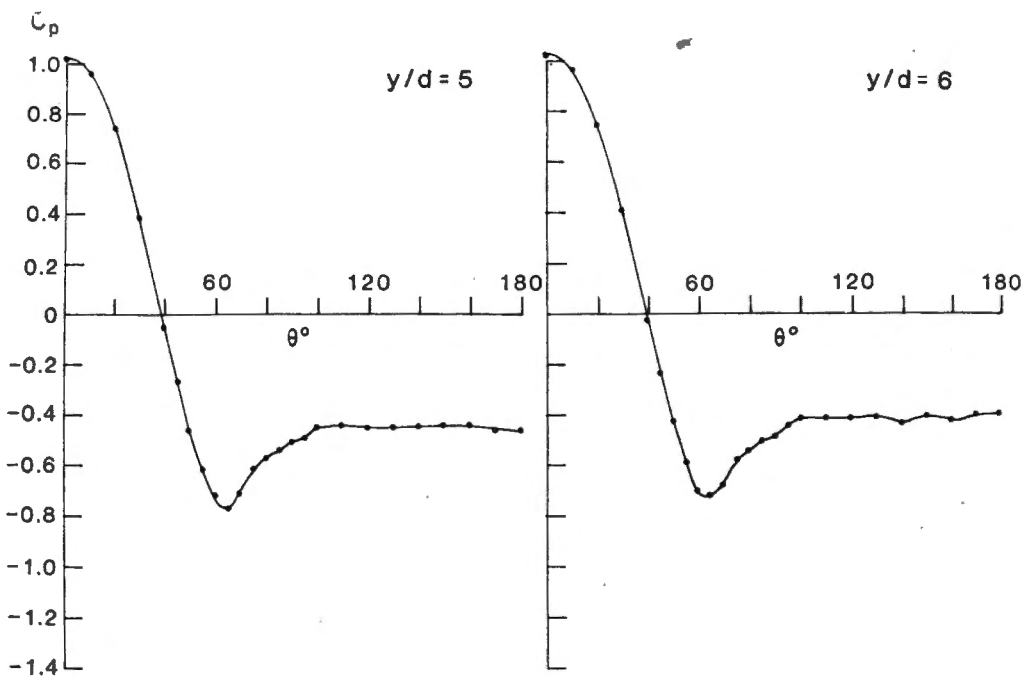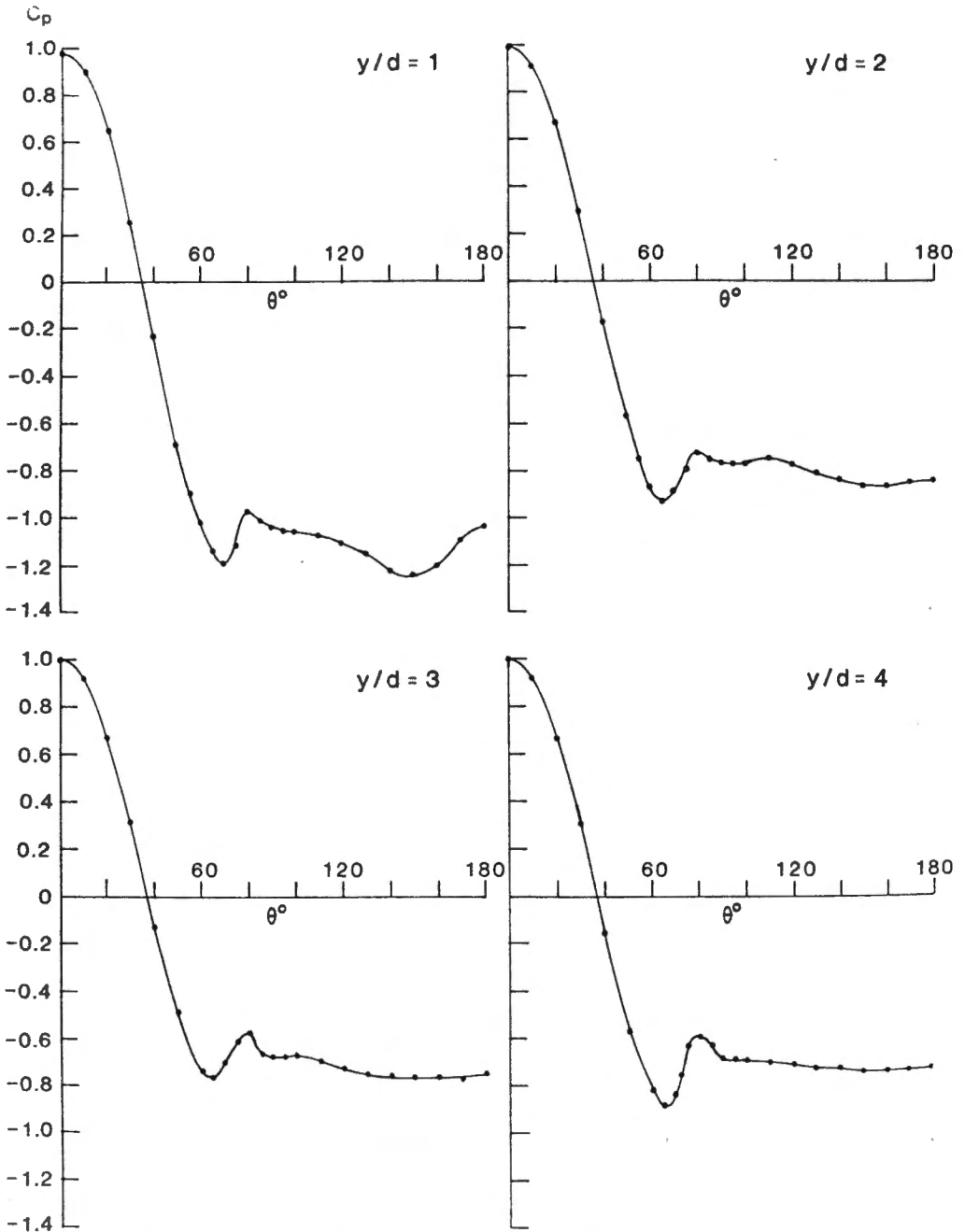
Figure A3: Circumferential distributions of the mean pressure coefficient measured on the cantilevered circular cylinder with an aspect ratio of 10.   41.
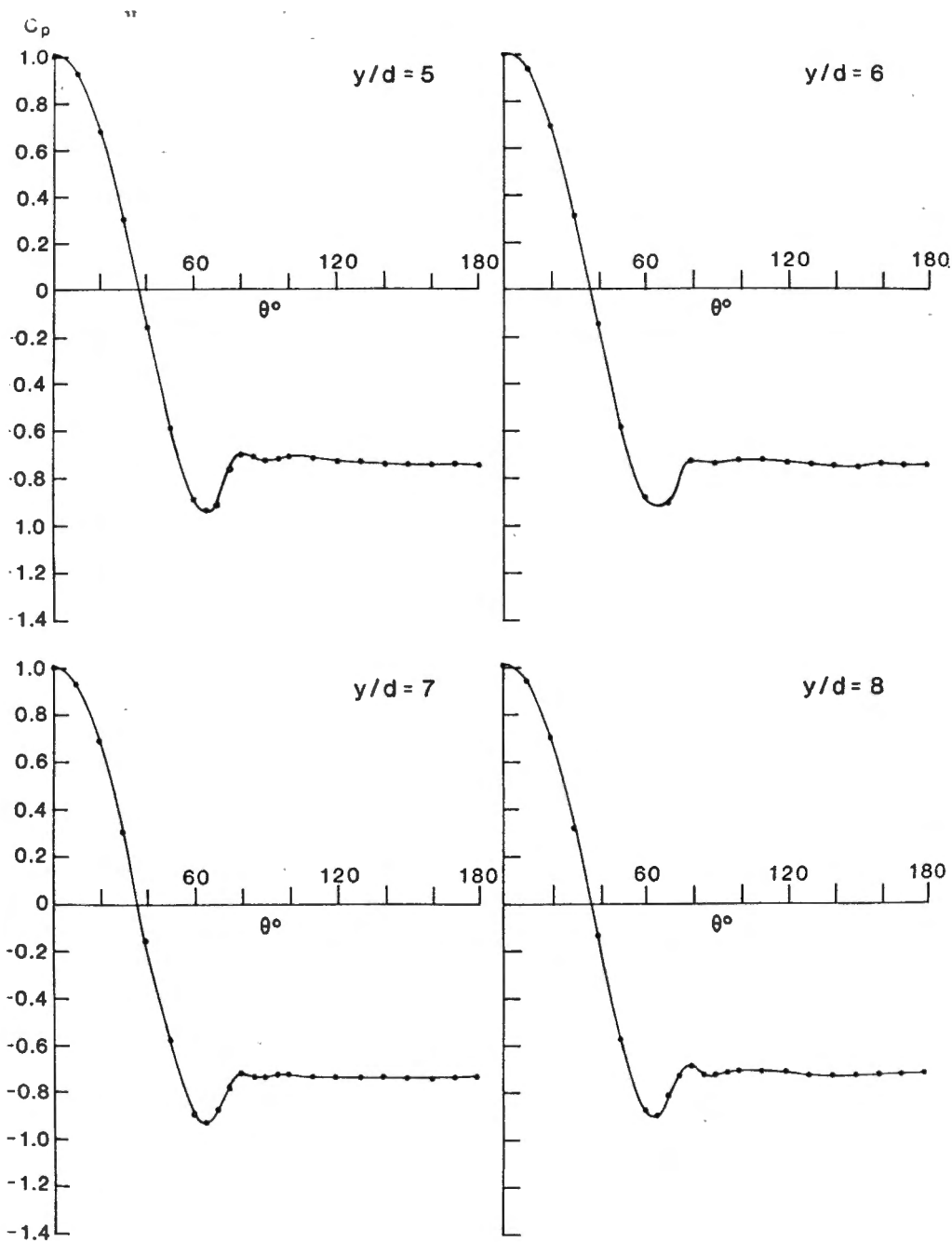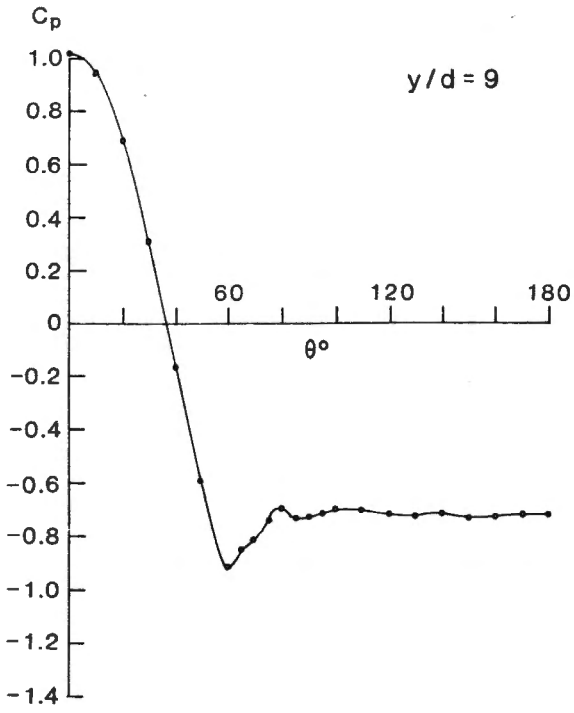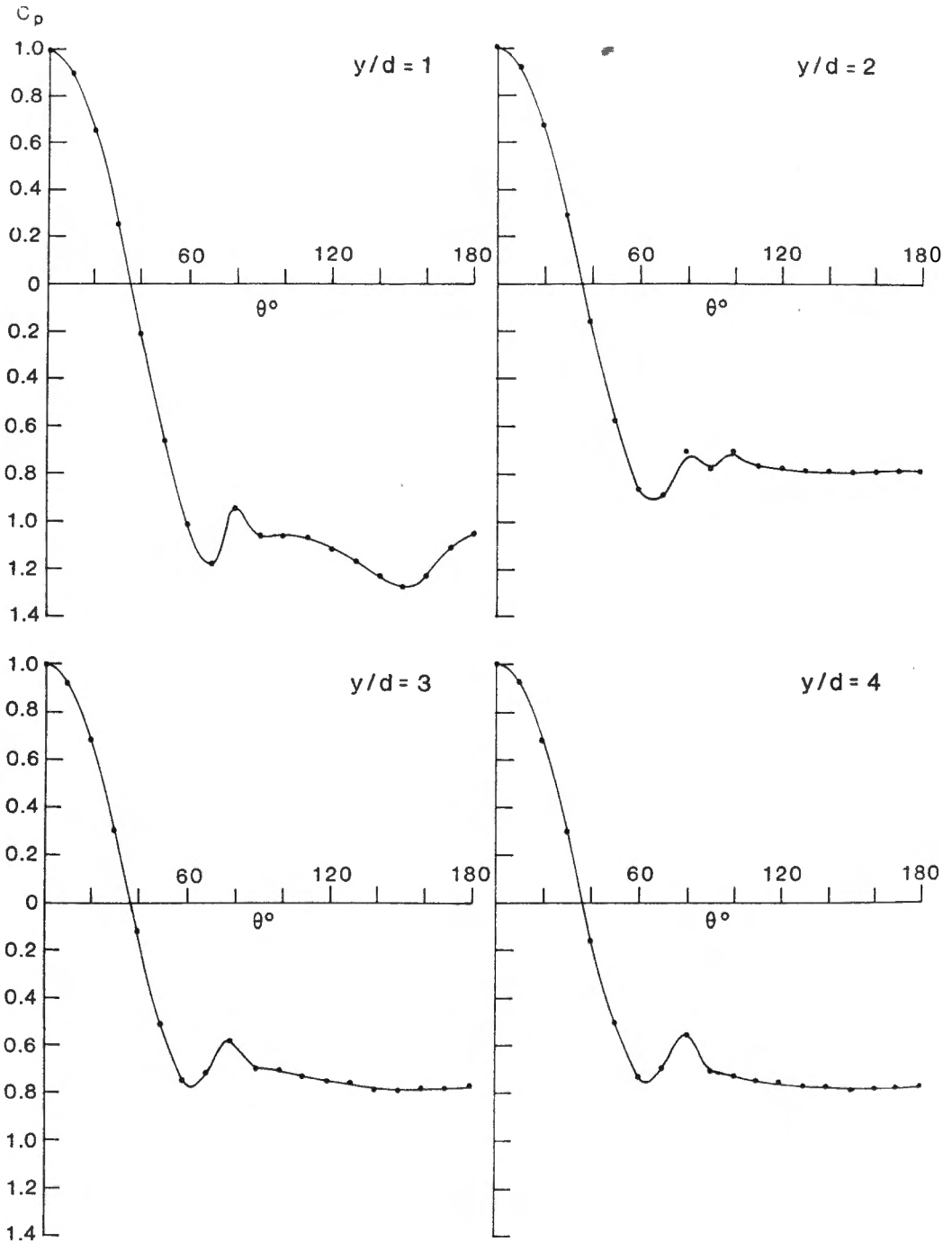
Figure A4: Circumferential distributions of the mean pressure coefficient measured on the cantilevered circular cylinder with an aspect ratio of 11.

44.
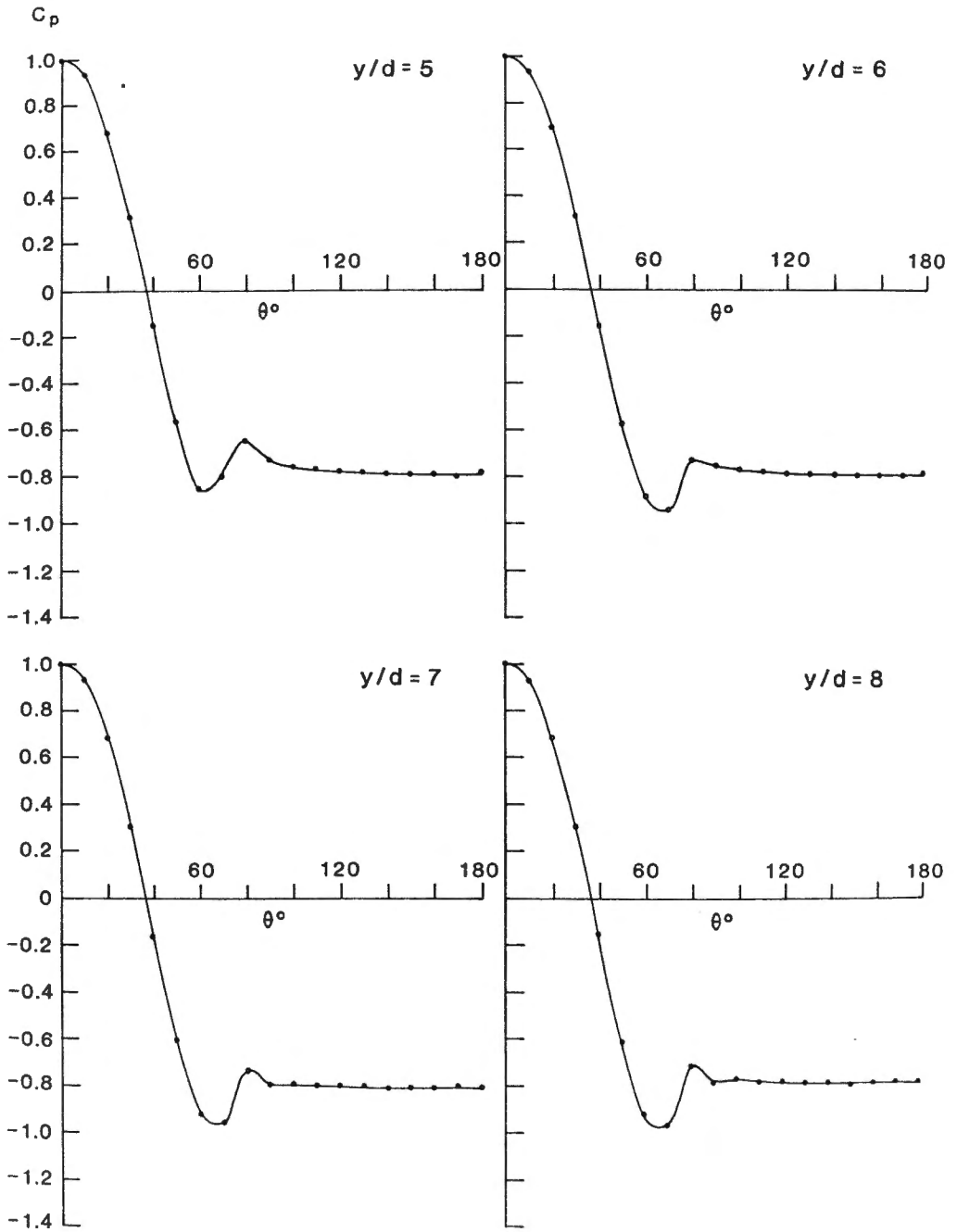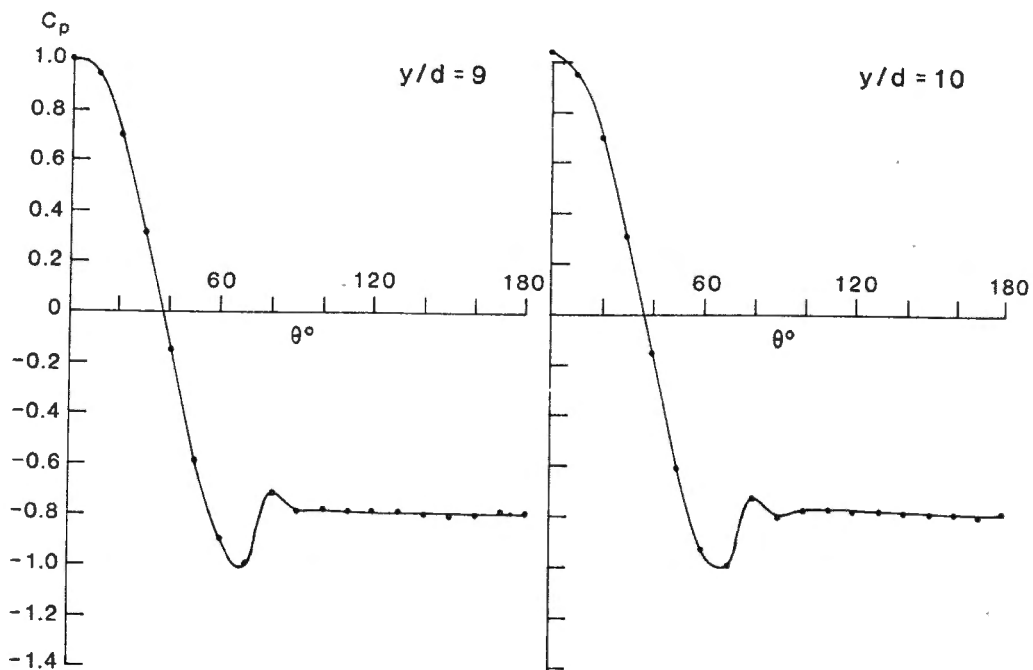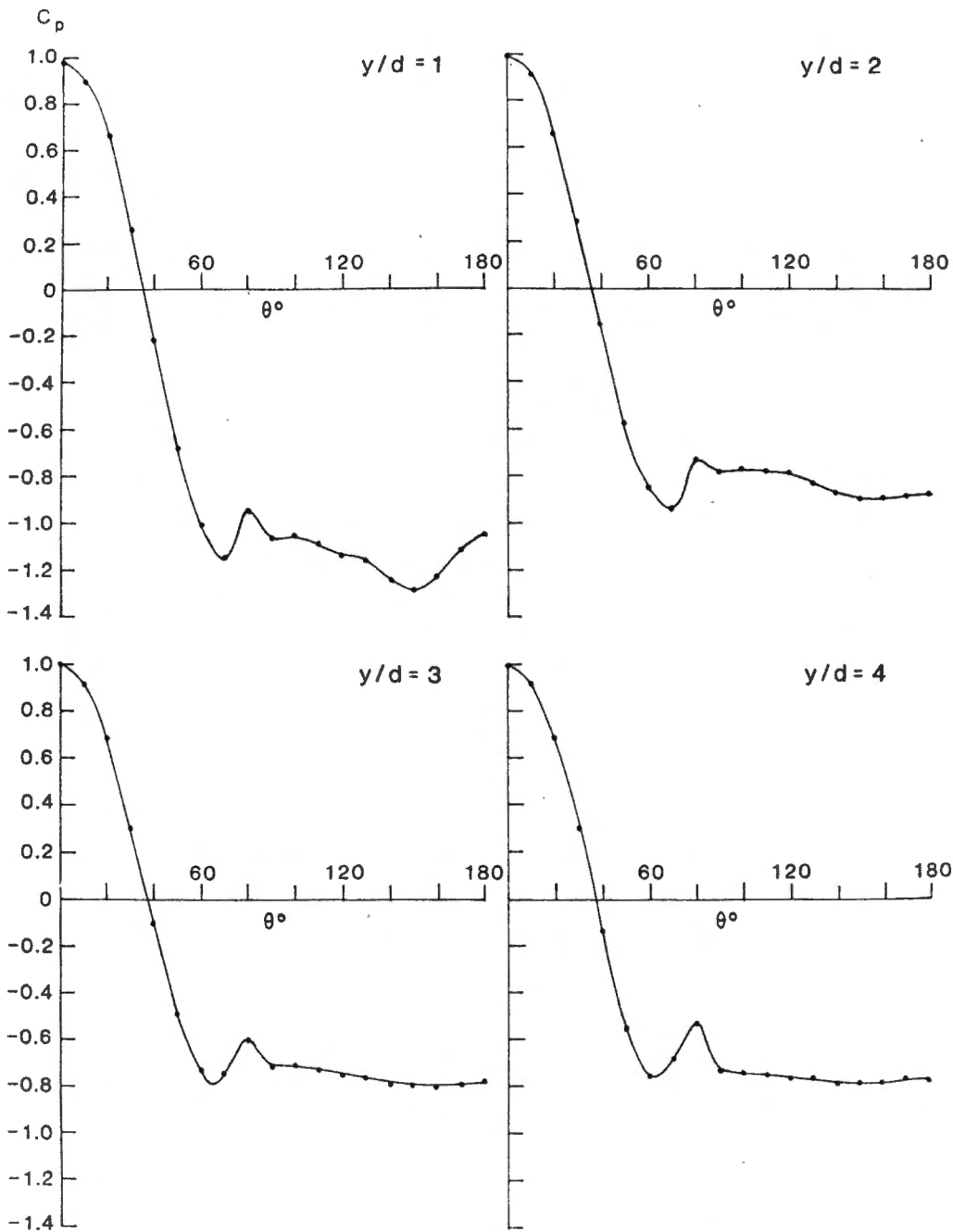
Figure A5: Circumferential distributions of the mean pressure coefficient measured on the cantilevered circular cylinder with an aspect ratio of 12.
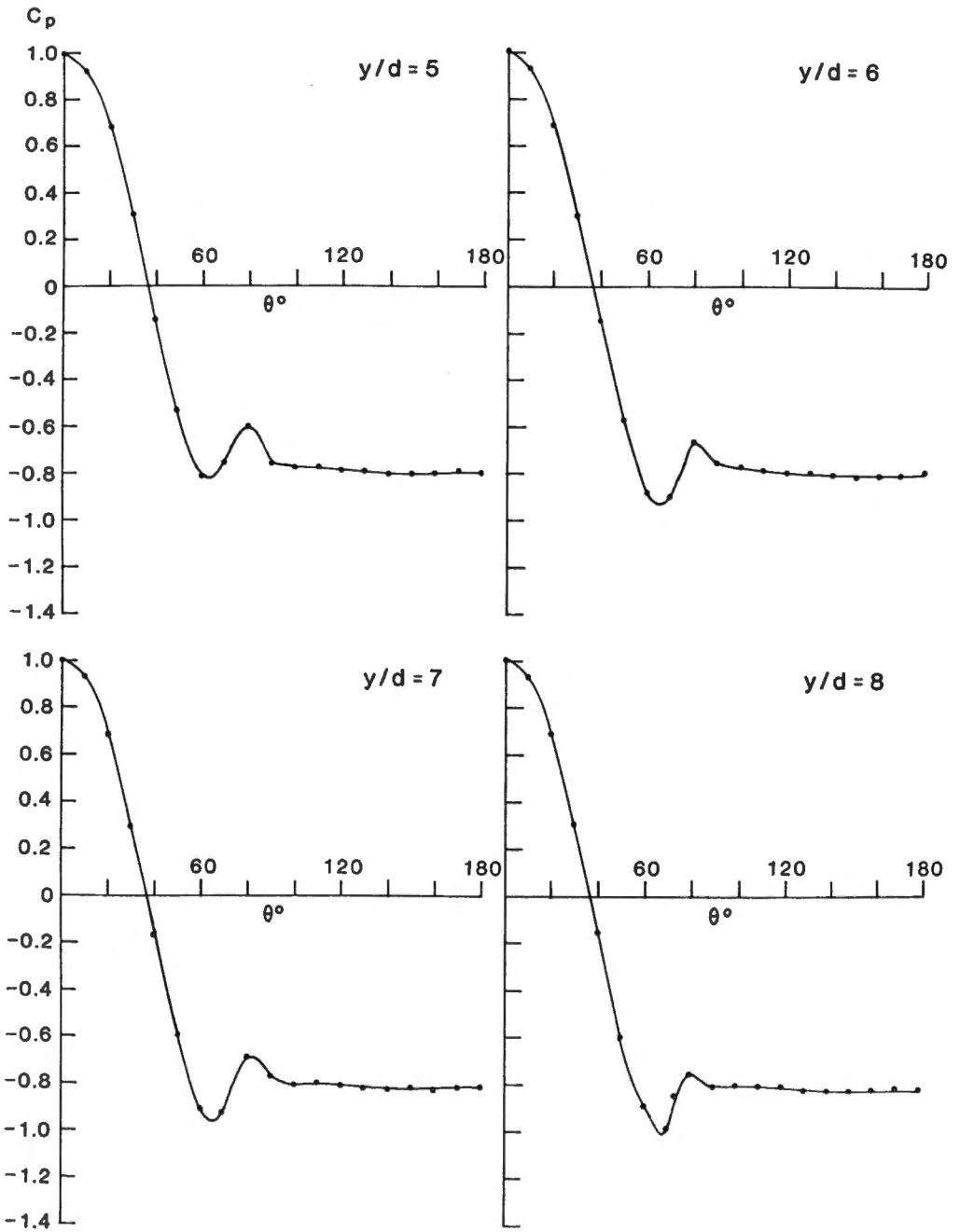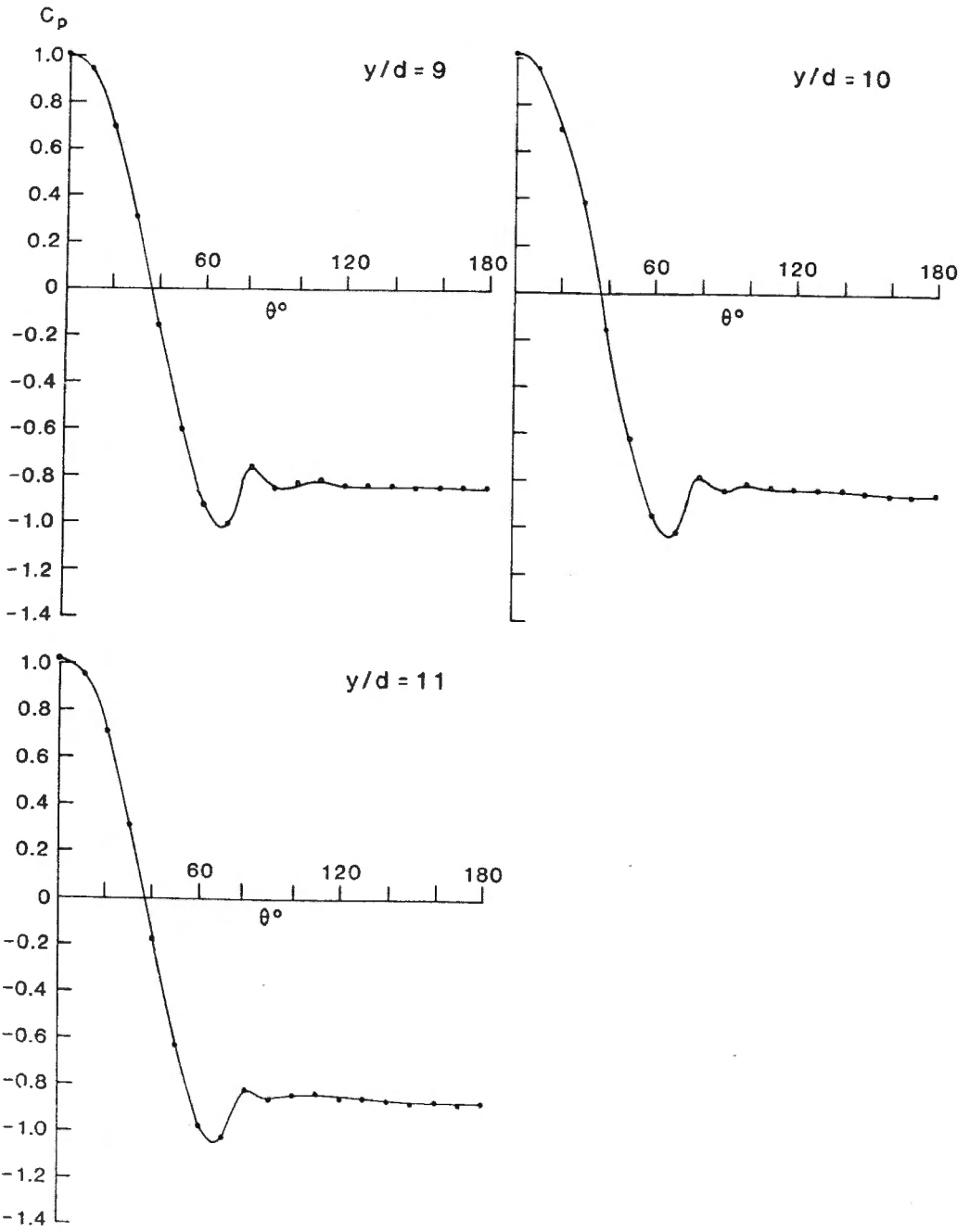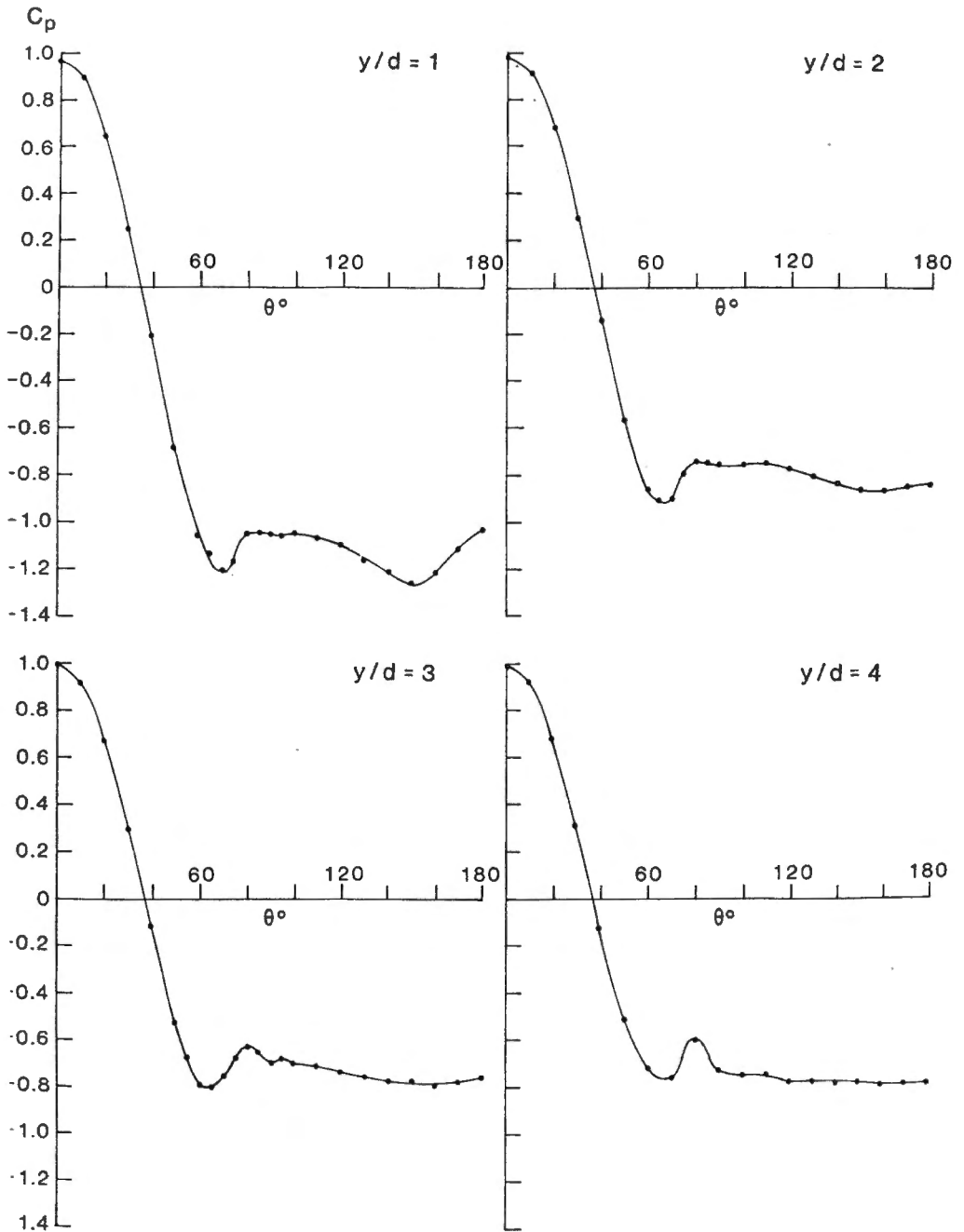
Figure A6: Circumferential distributions of the mean pressure coefficient measured on the cantilevered circular cylinder with an aspect ratio of 13.

50.
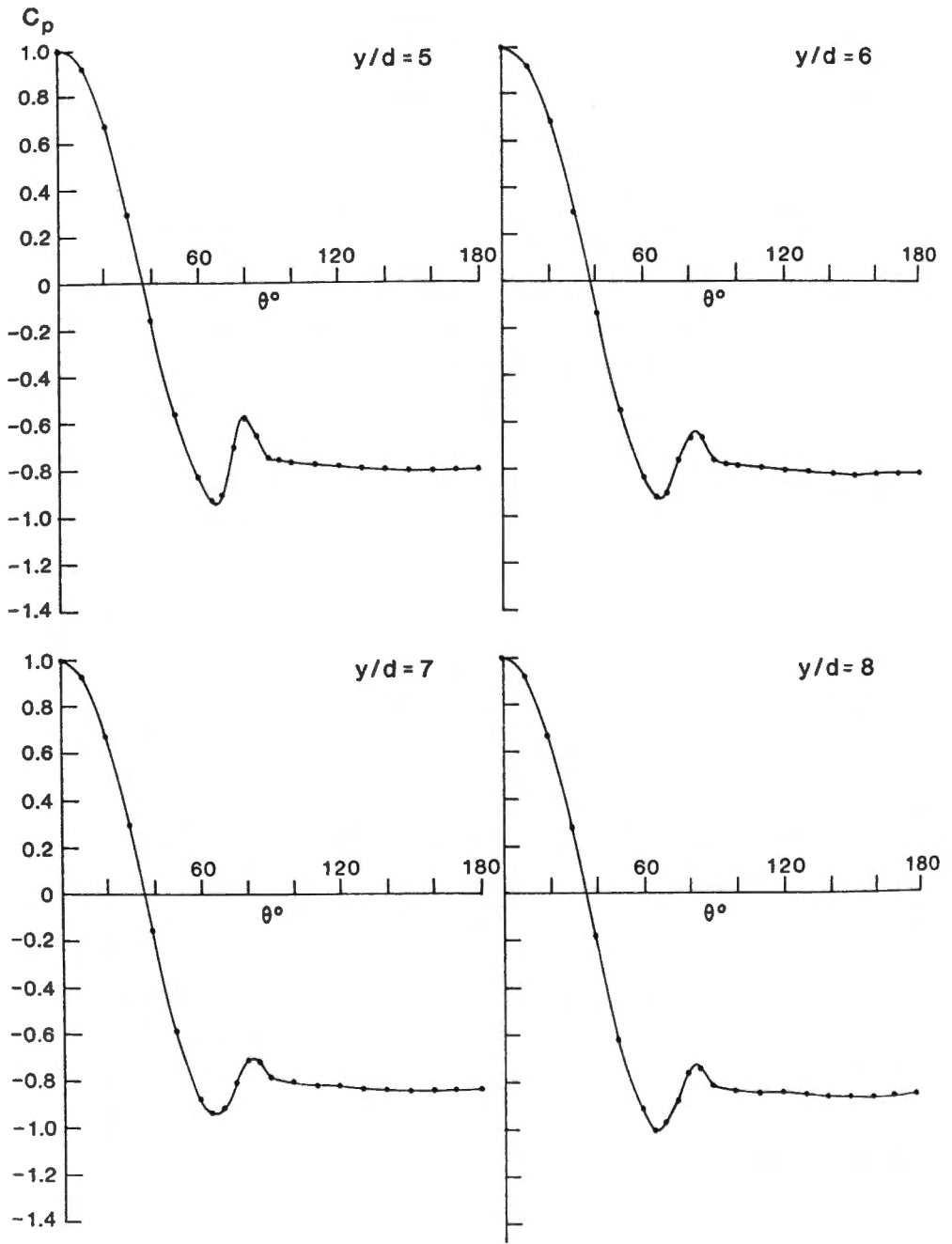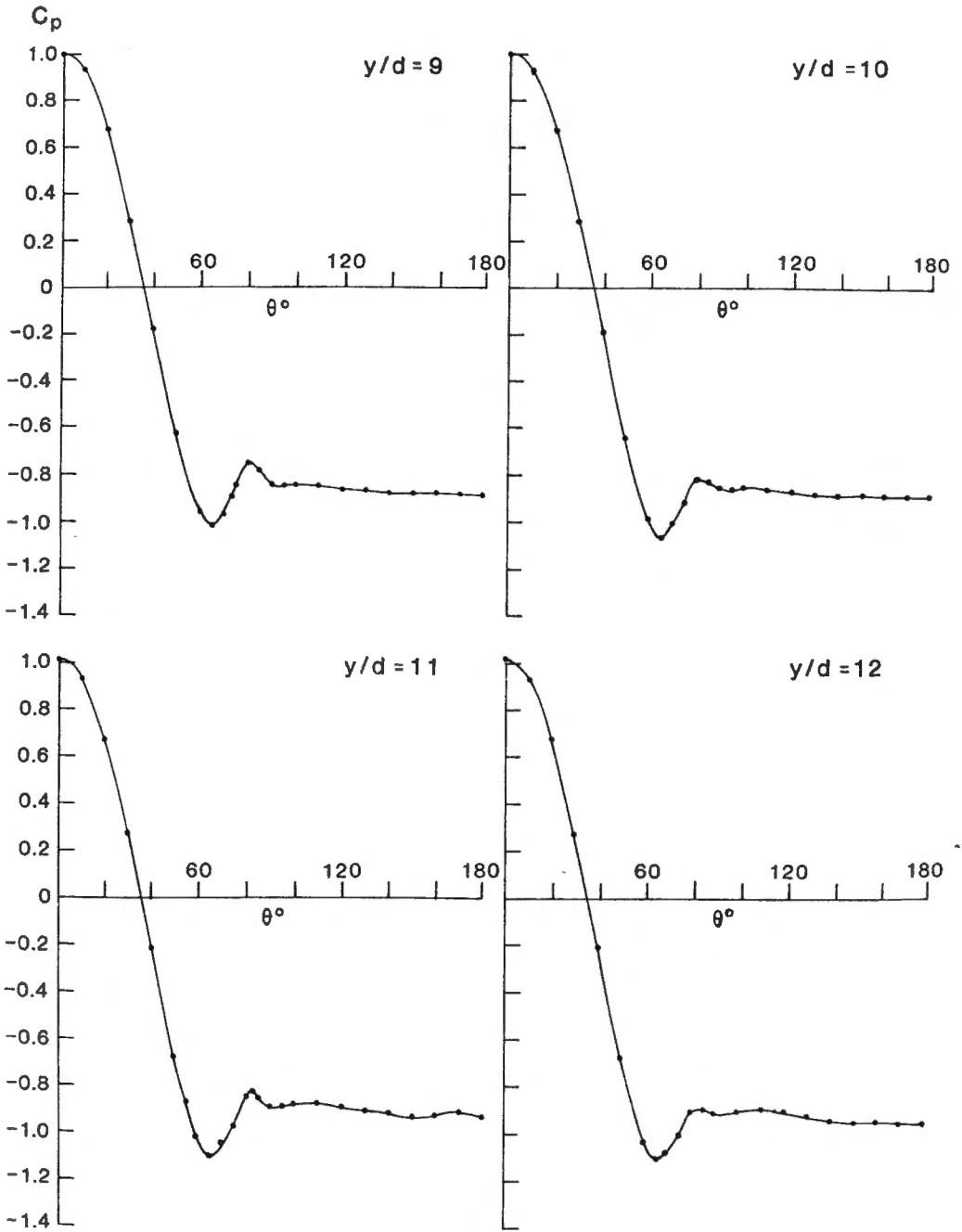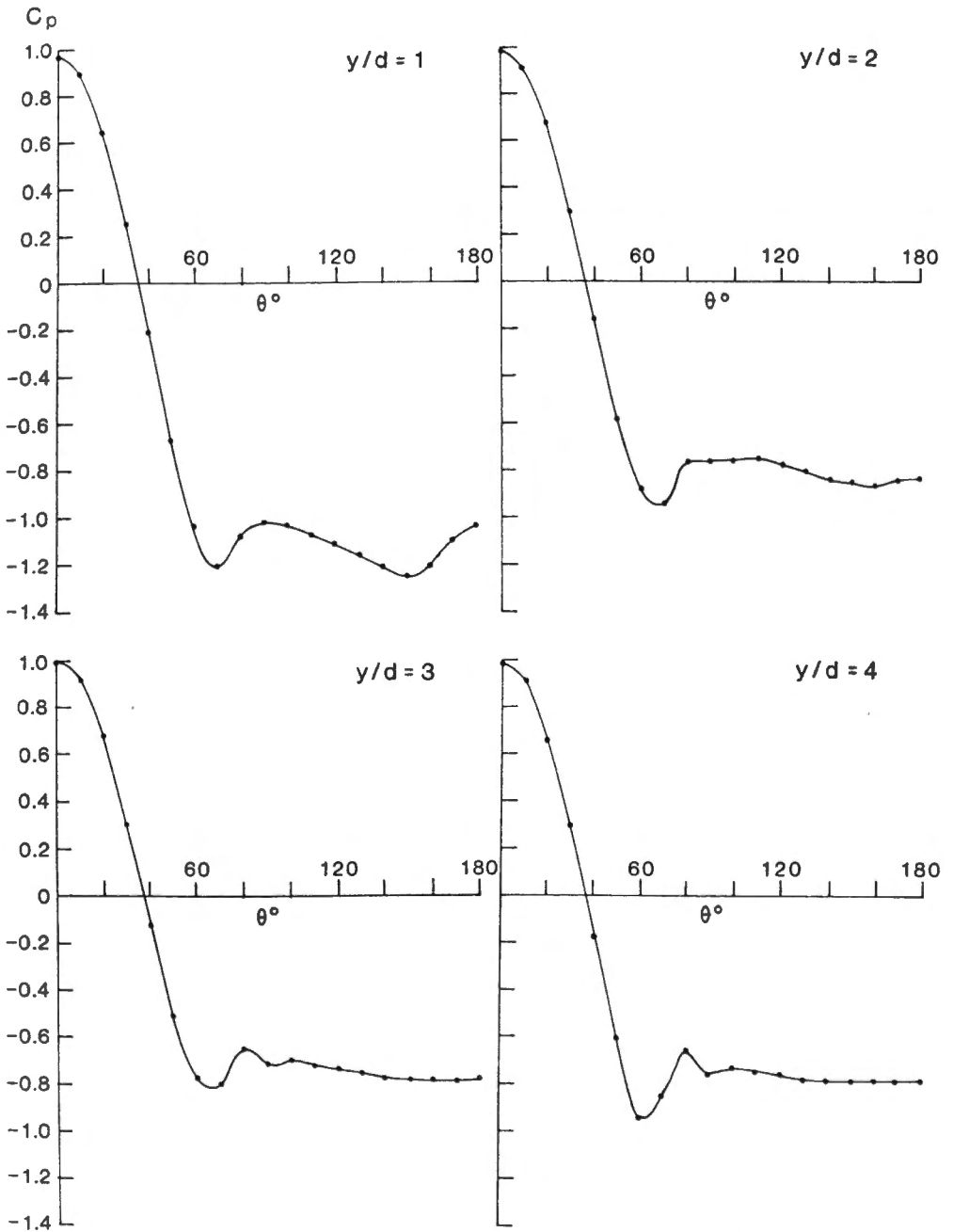
Figure A7: Circumferential distributions of the mean pressure coefficient measured on the cantilevered circular cylinder with an aspect ratio of 16.
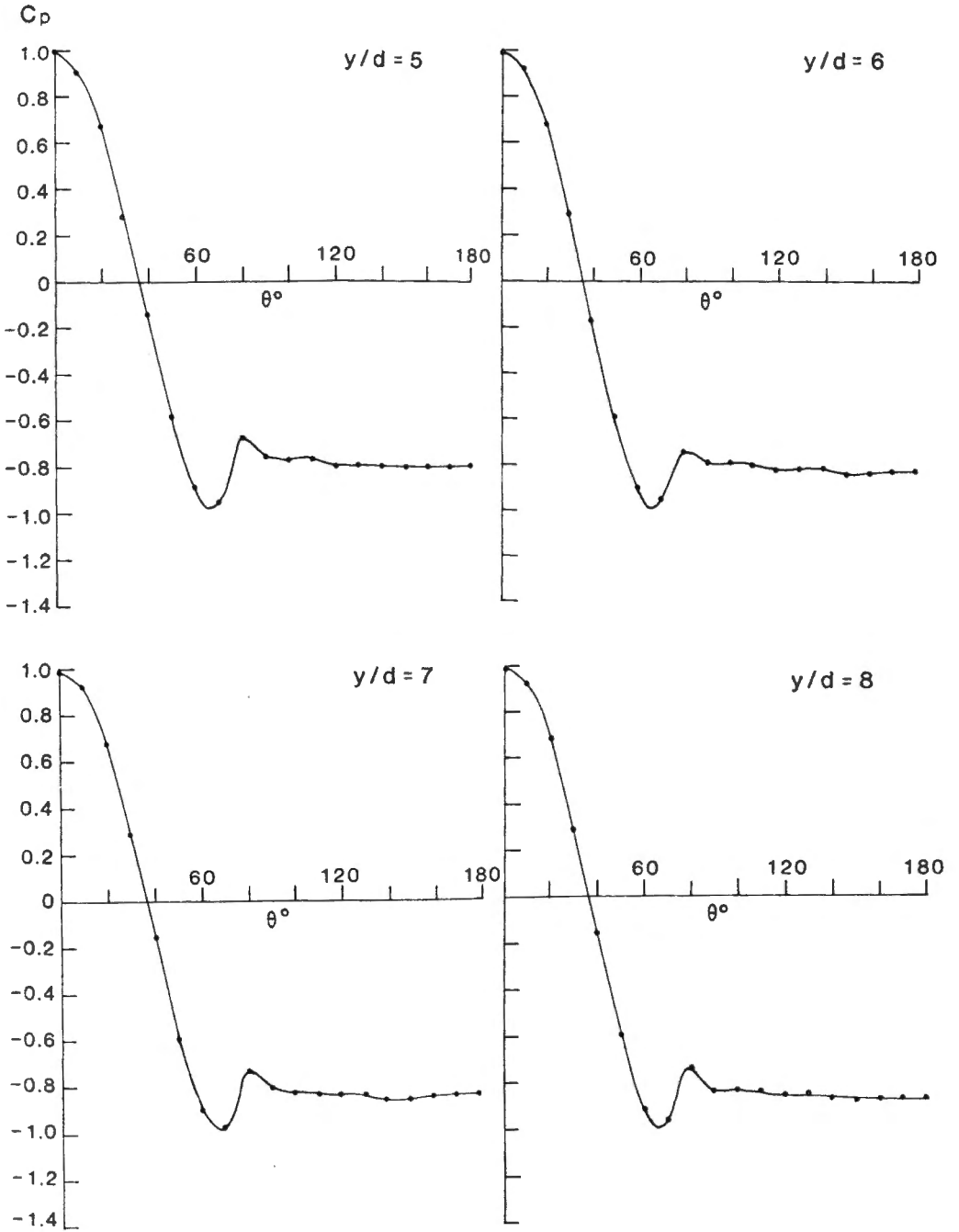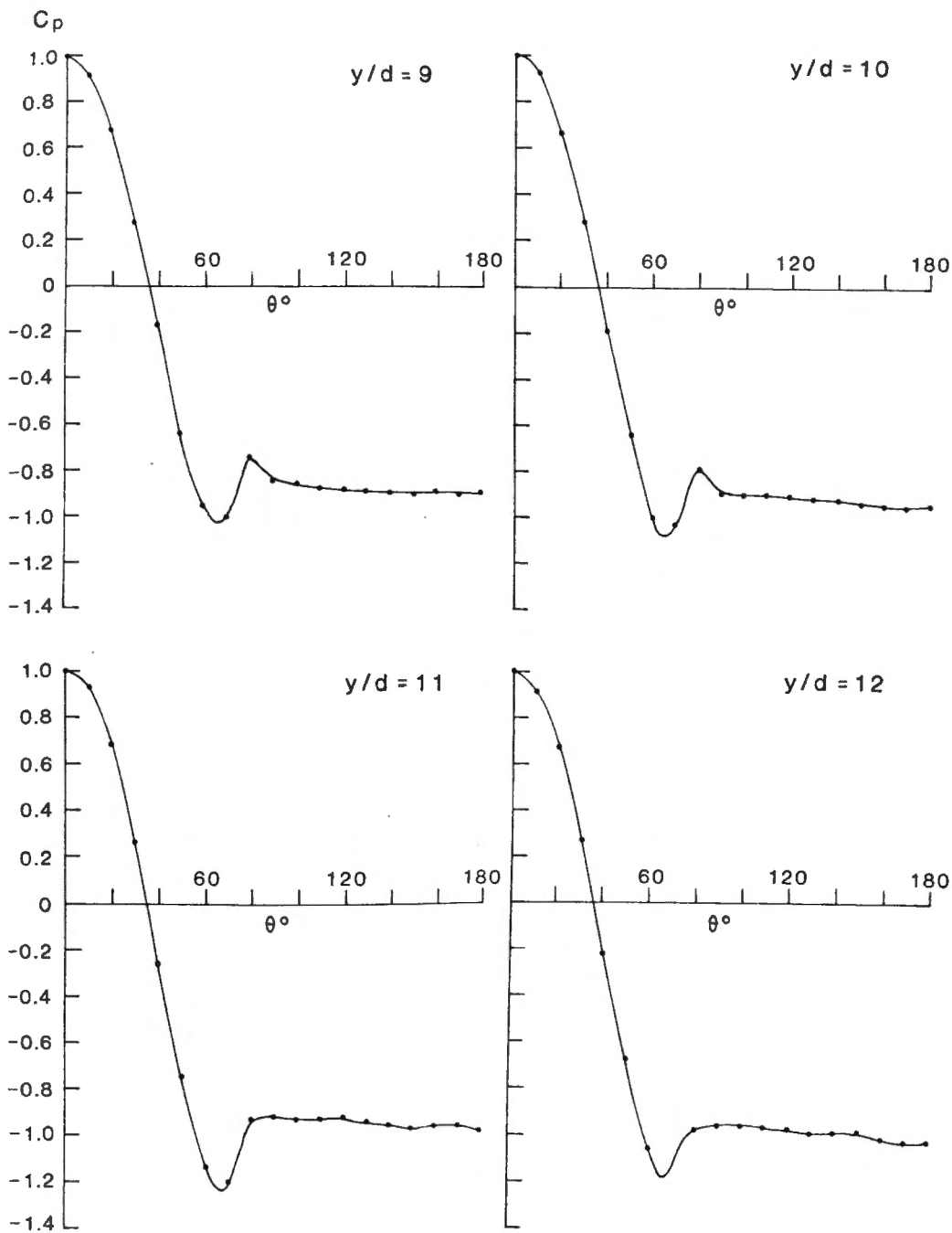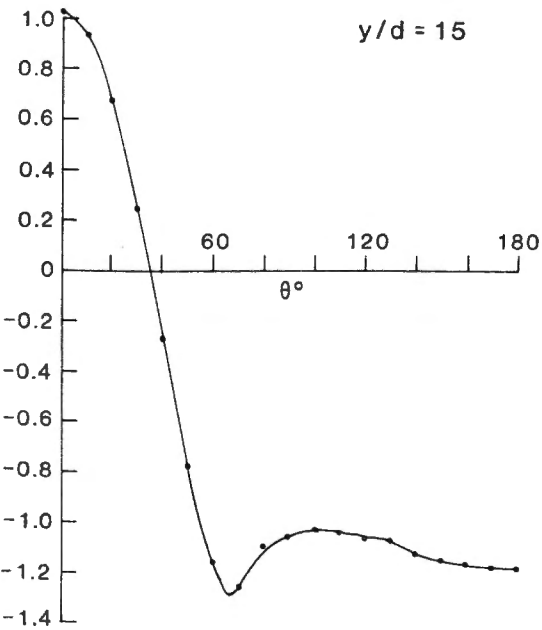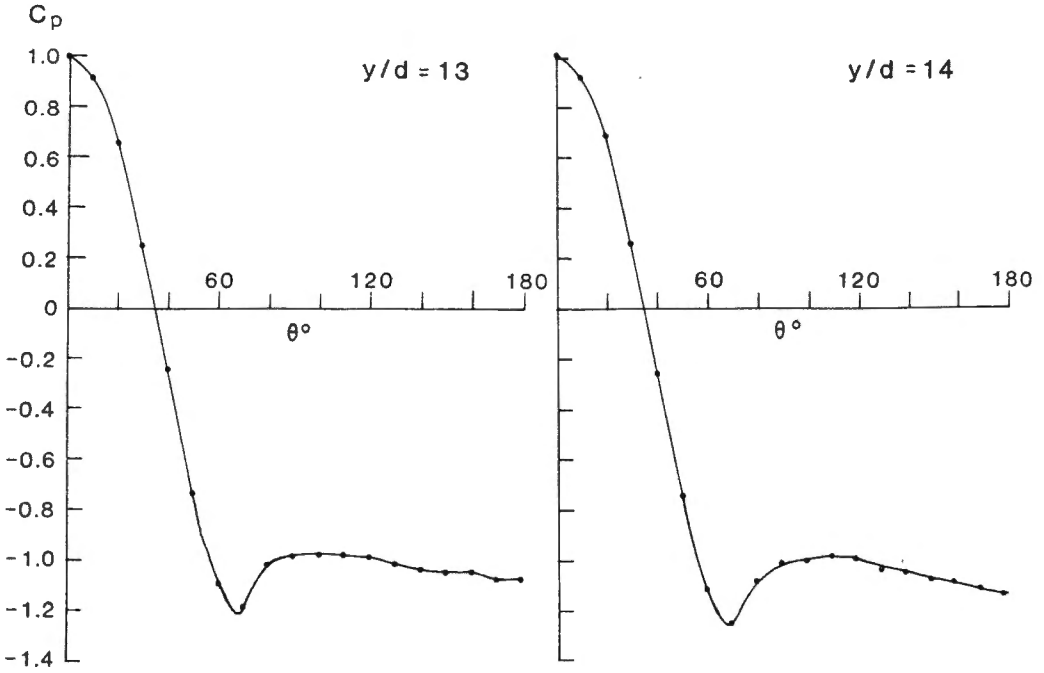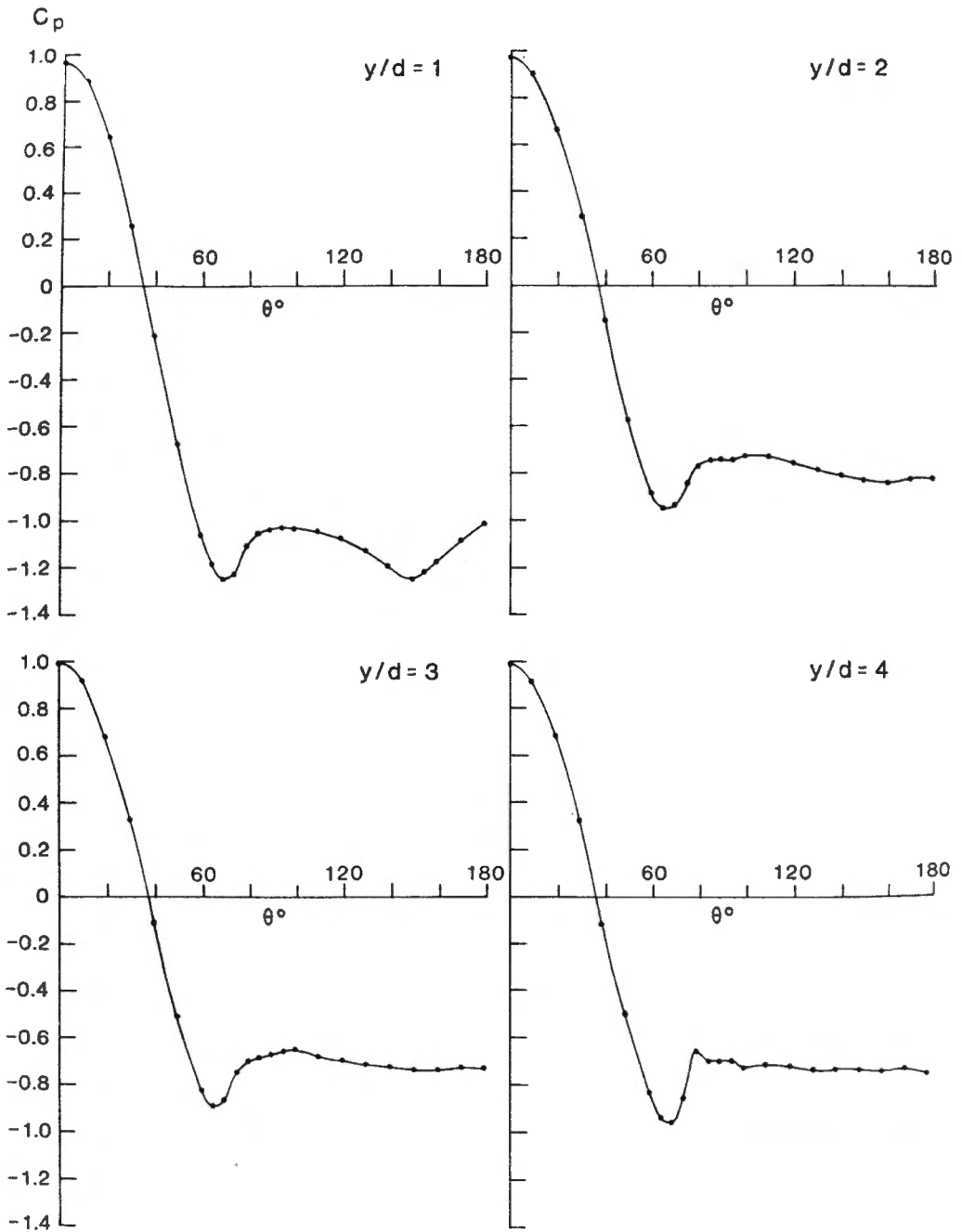
Figure A8: Circumferential distributions of the mean pressure coefficient measured on the cantilevered circular cylinder with an aspect ratio of 19.
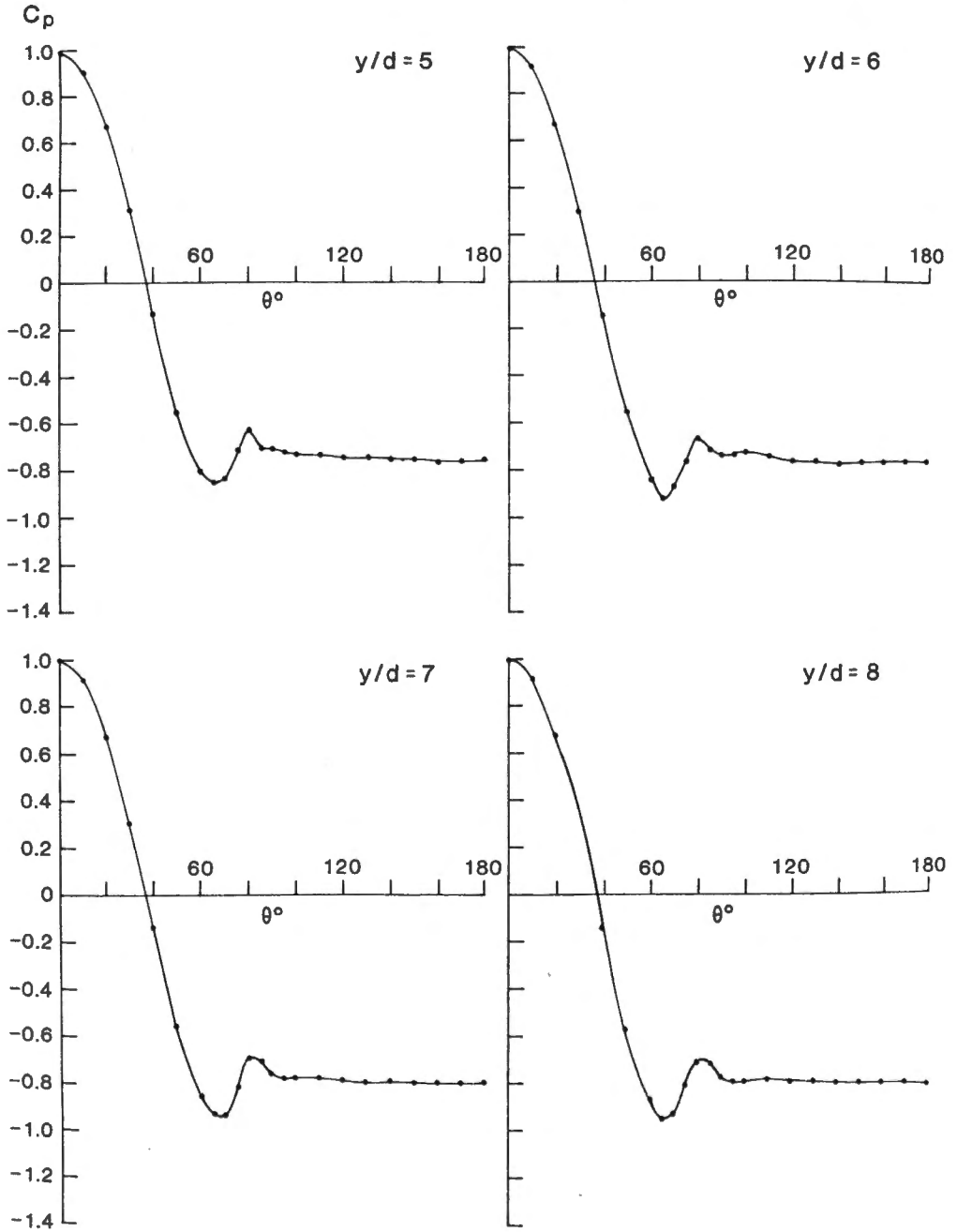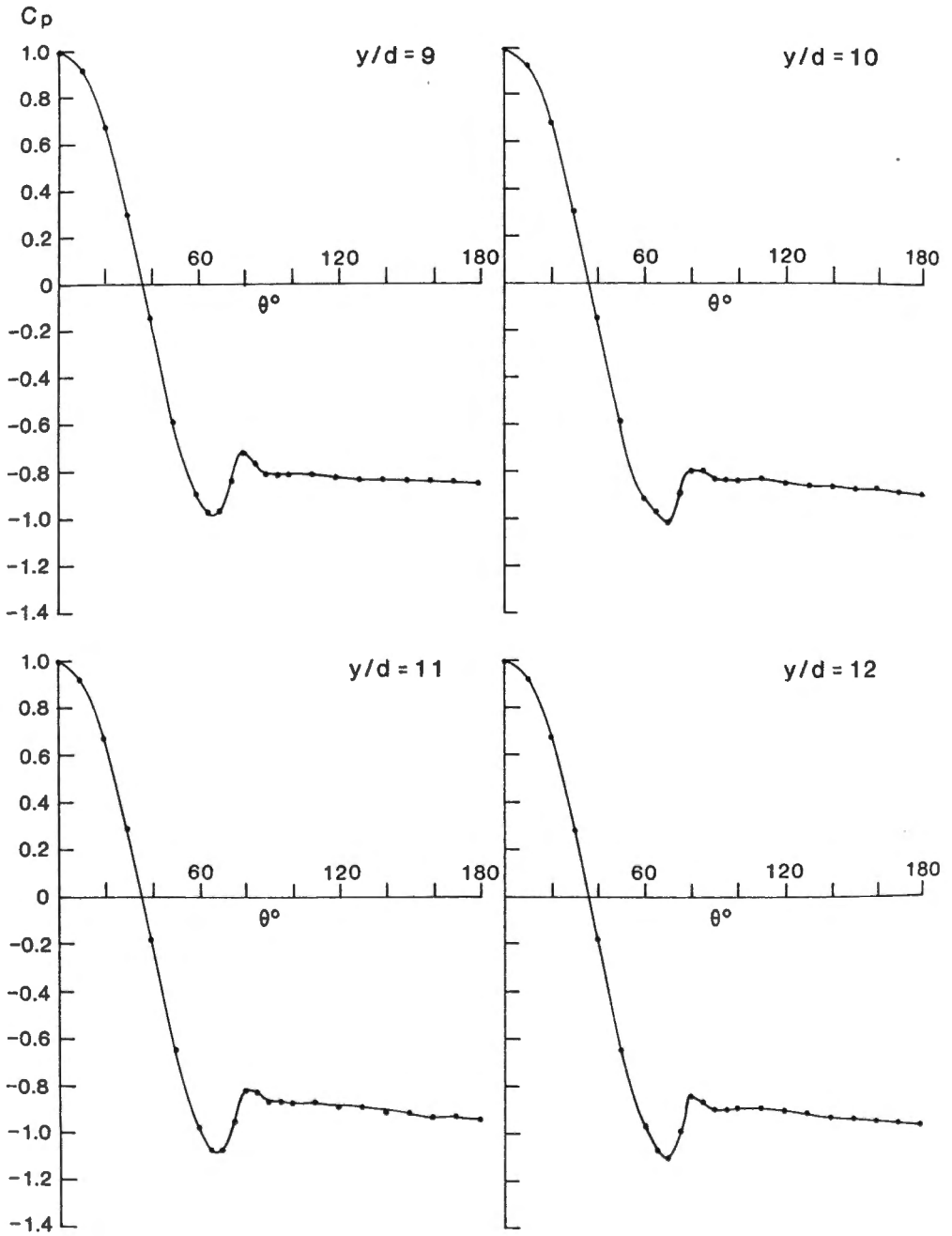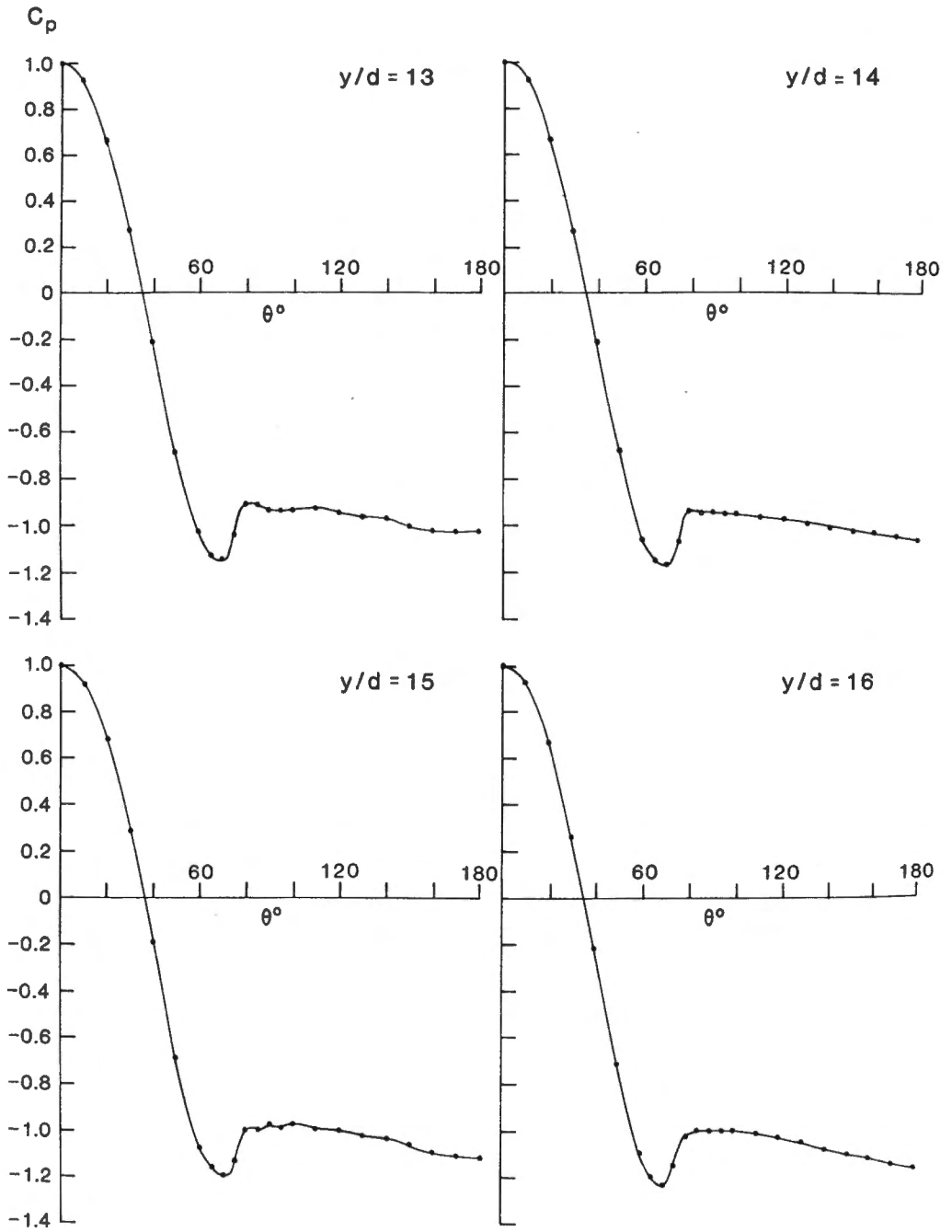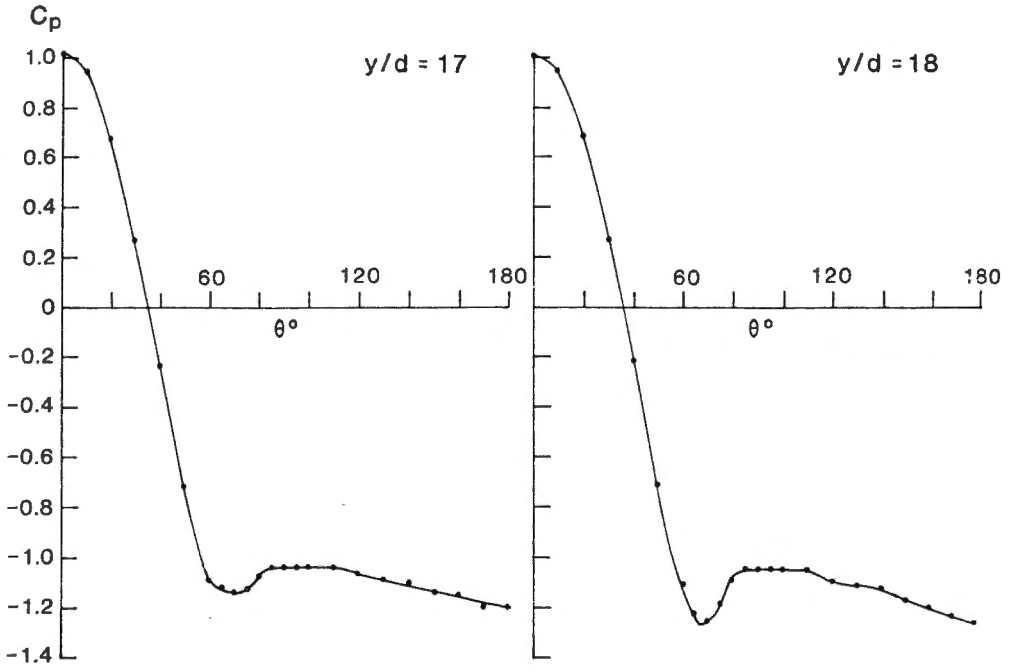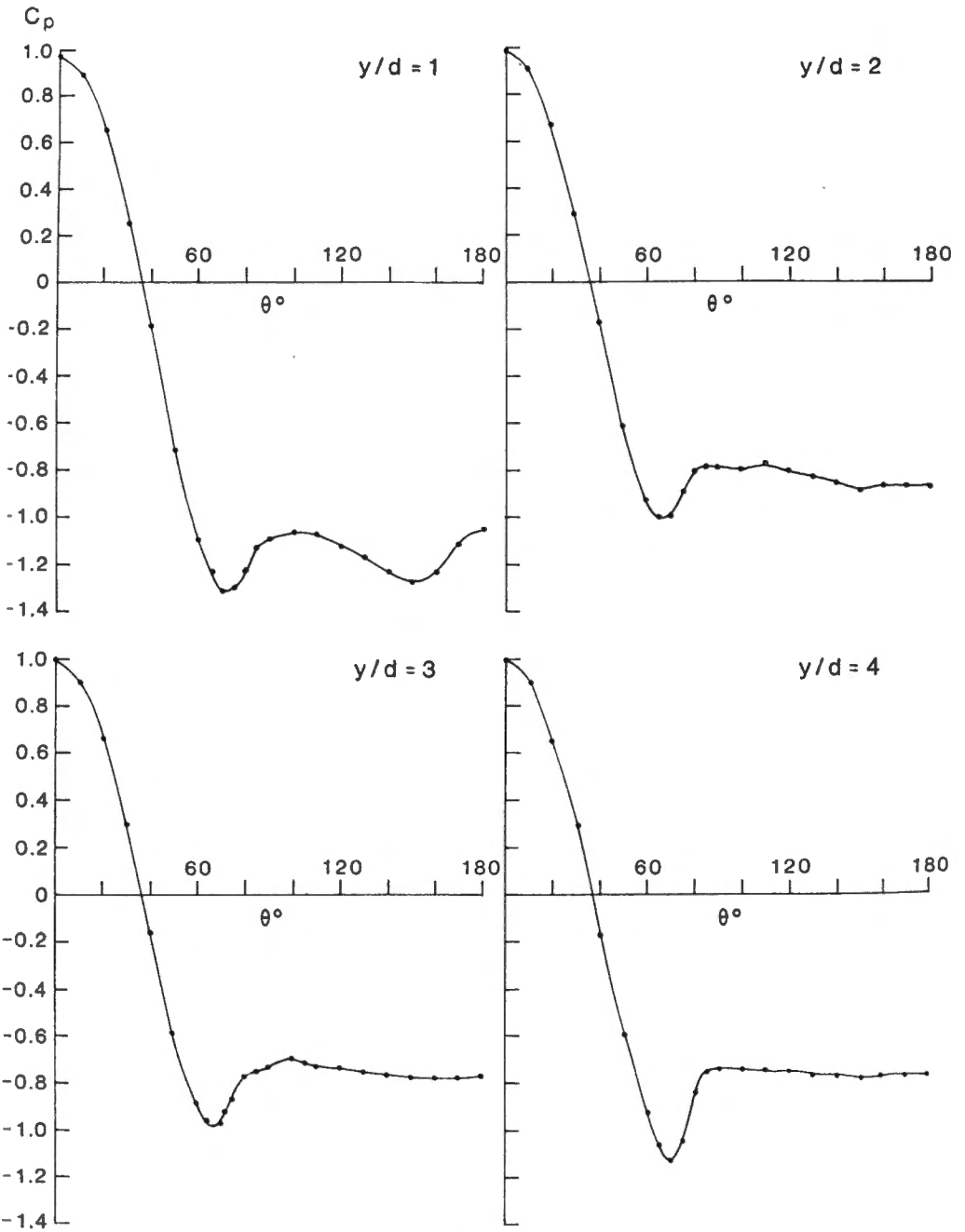
Figure A9: Circumferential distributions of the mean pressure coefficient measured on the cantilevered circular cylinder with an aspect ratio of 25.
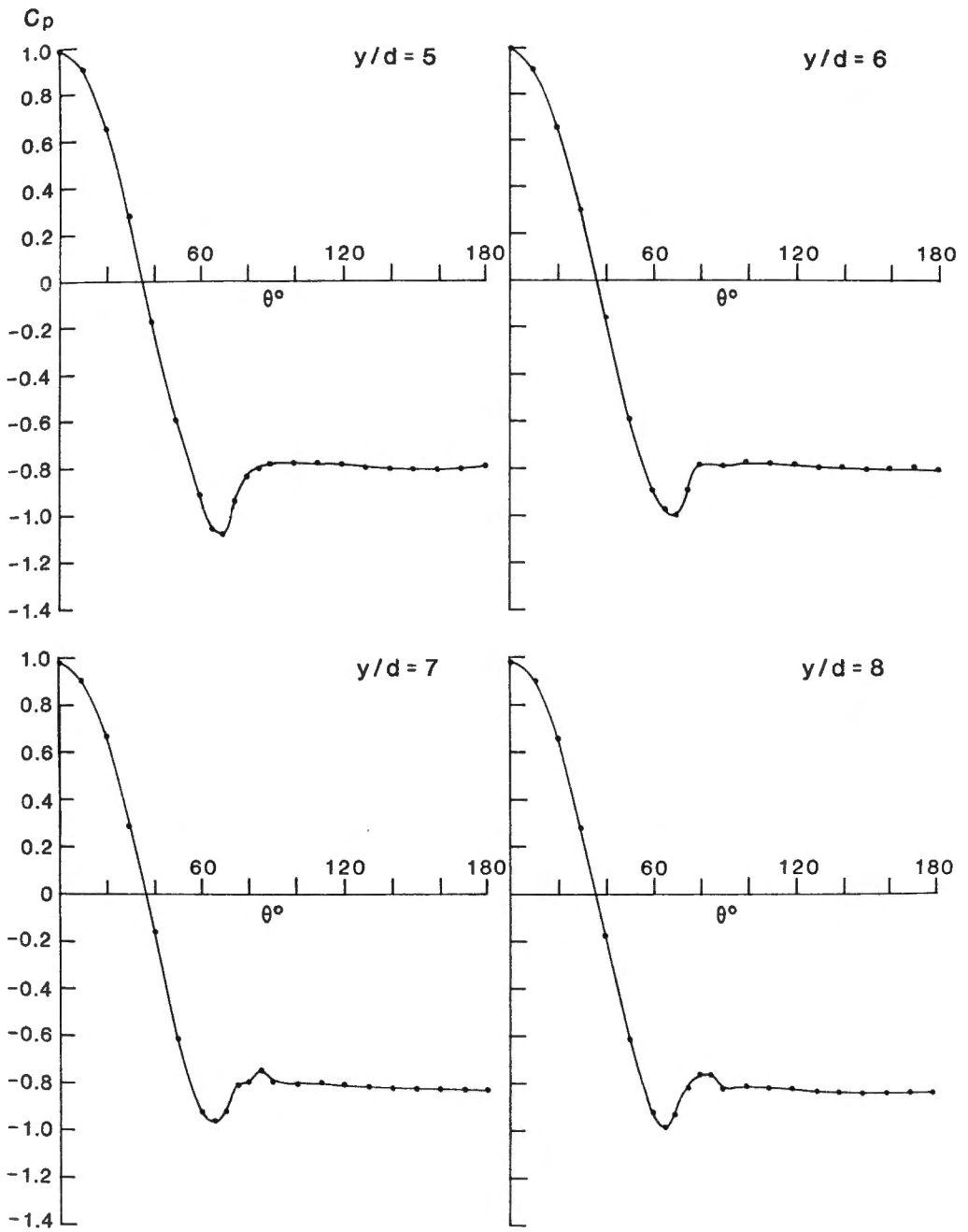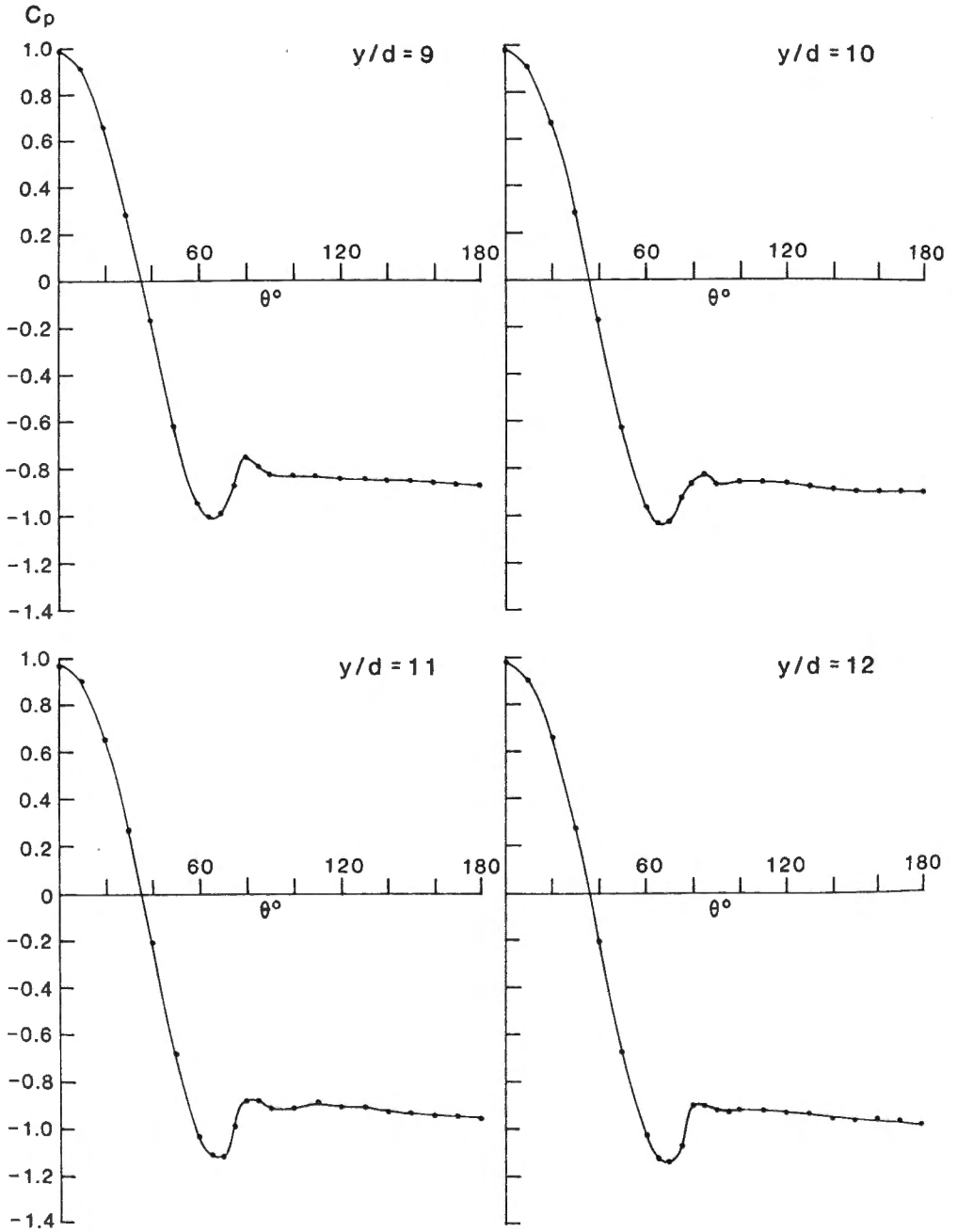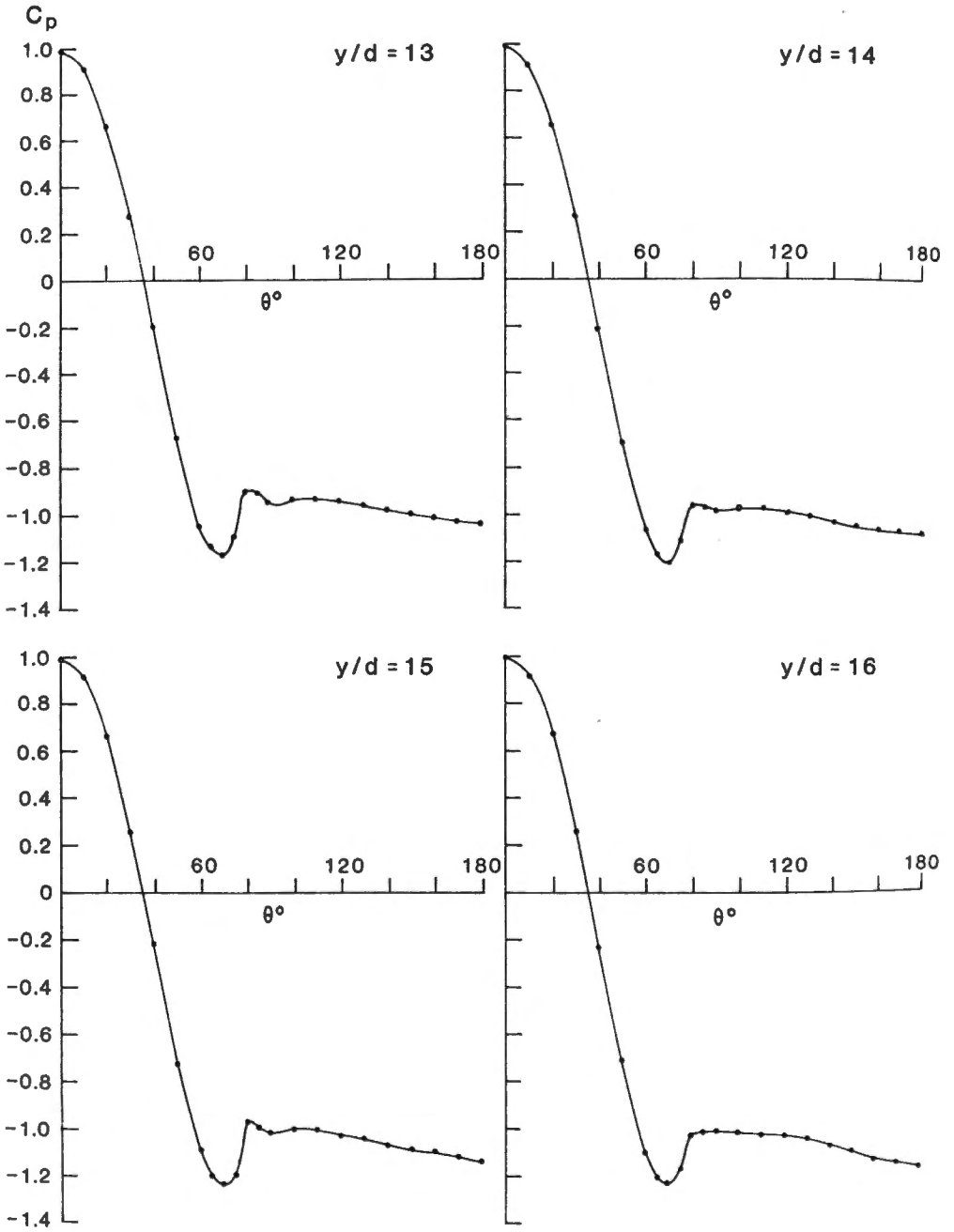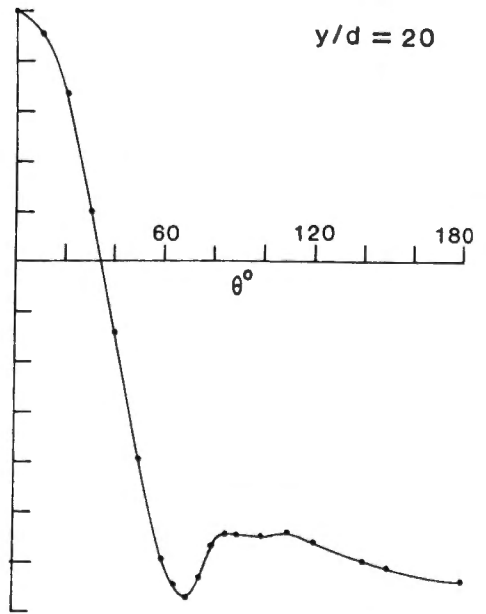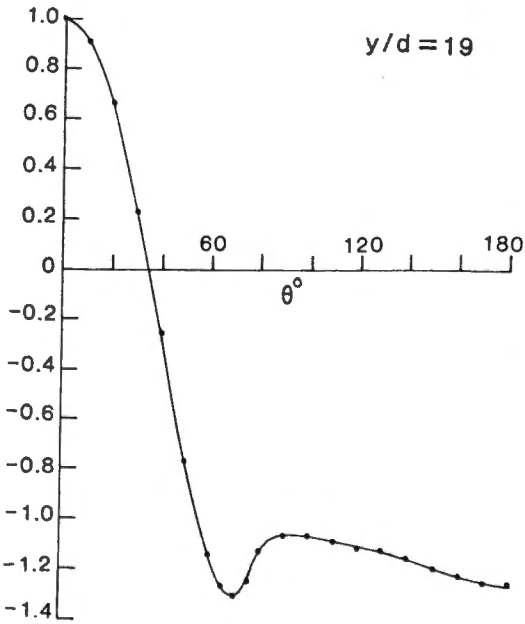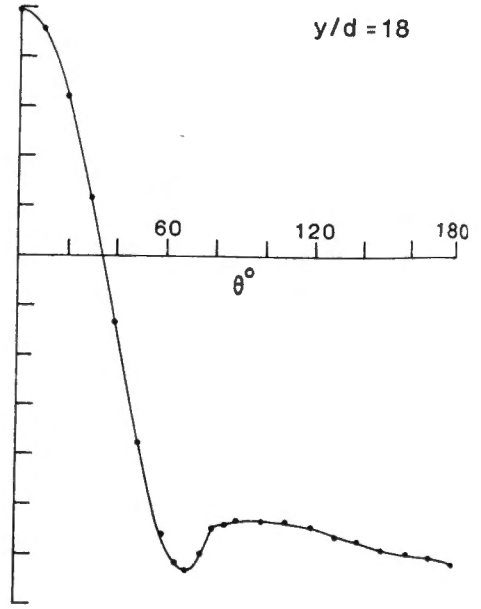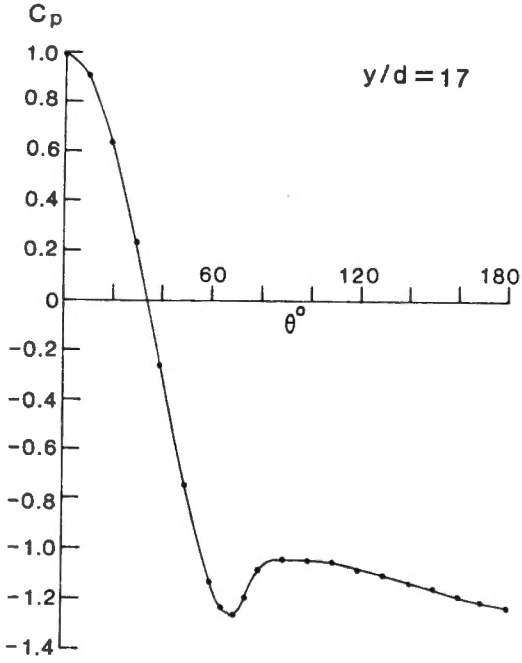
Figure A10: Circumferential distributions of the mean pressure coefficient measured on the cantilevered circular cylinder with an aspect ratio of 30.
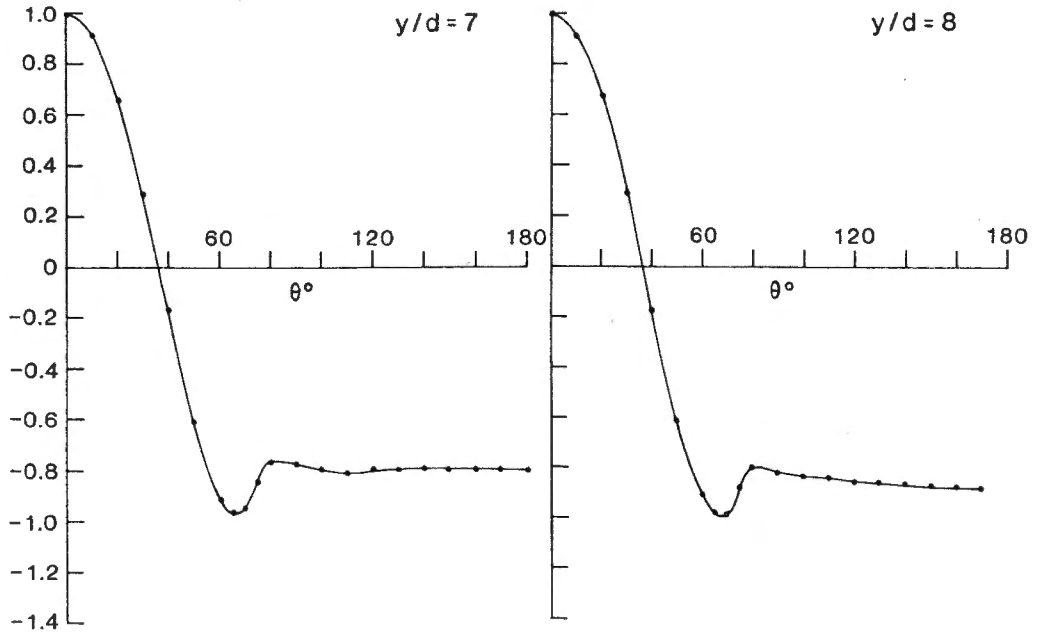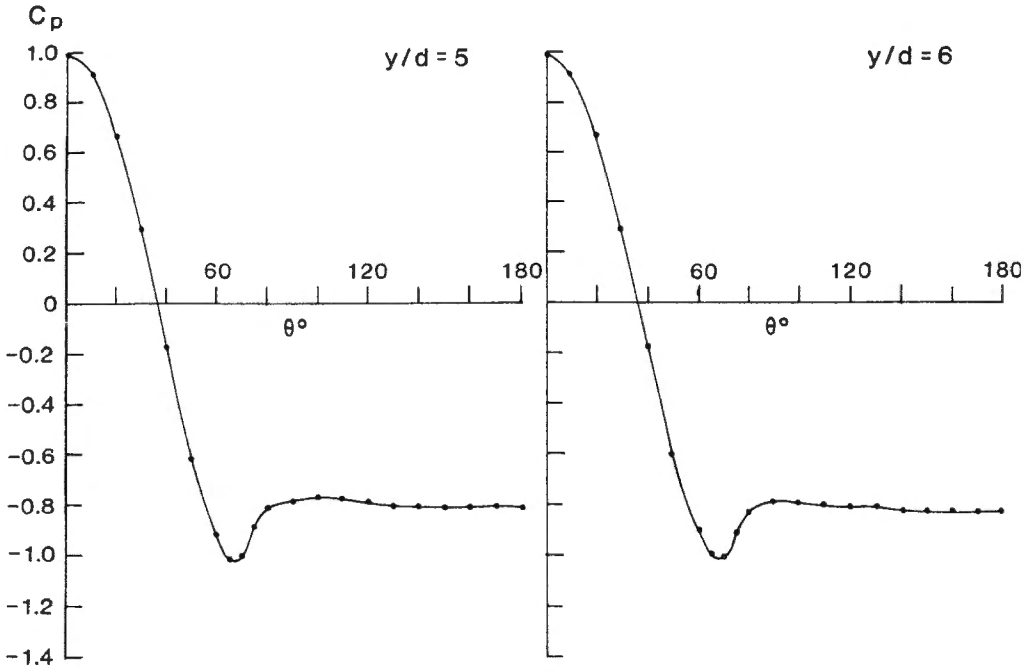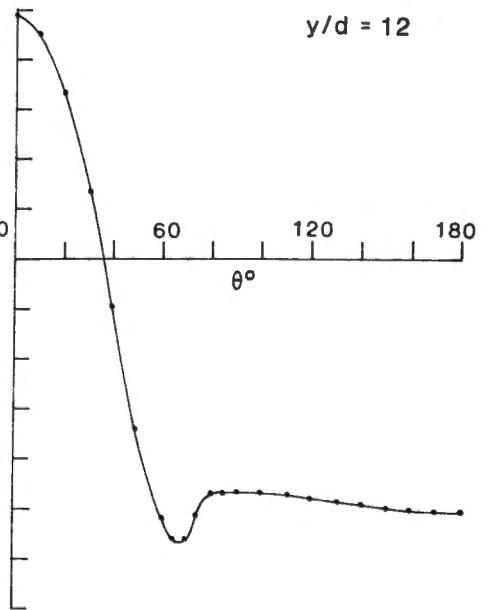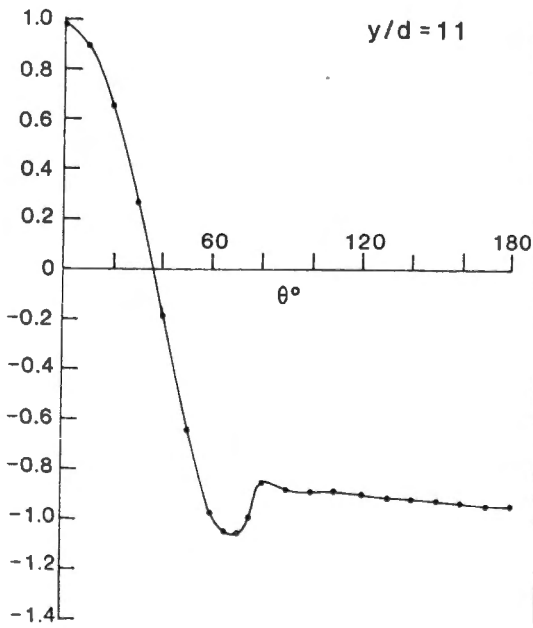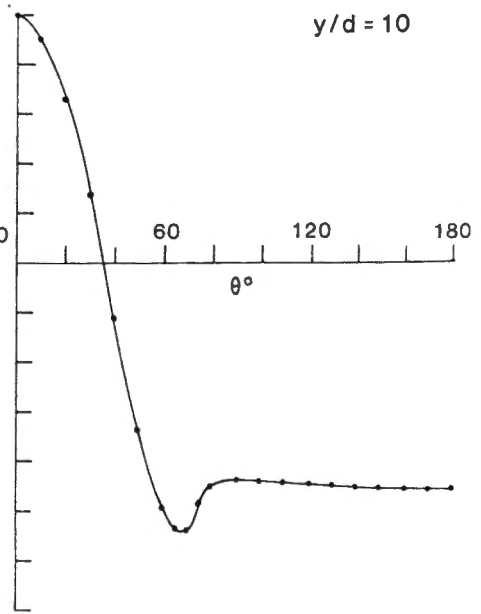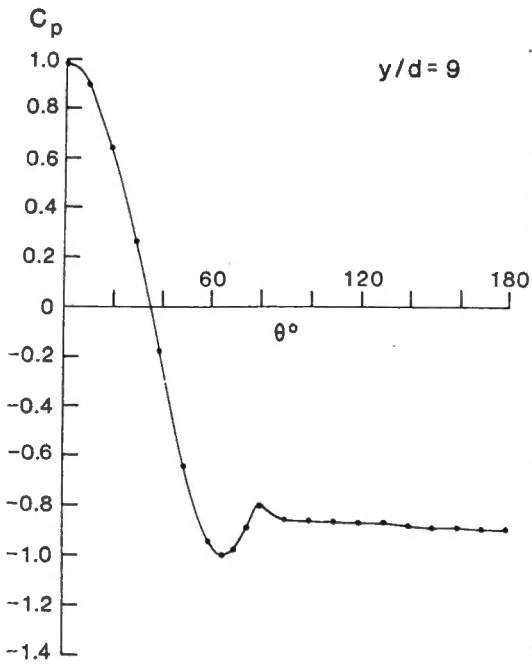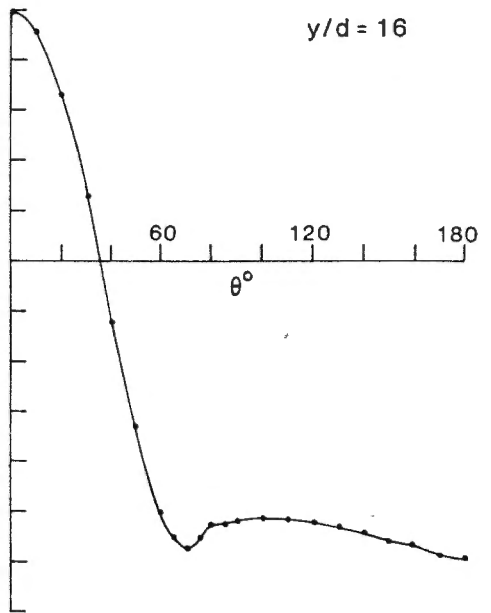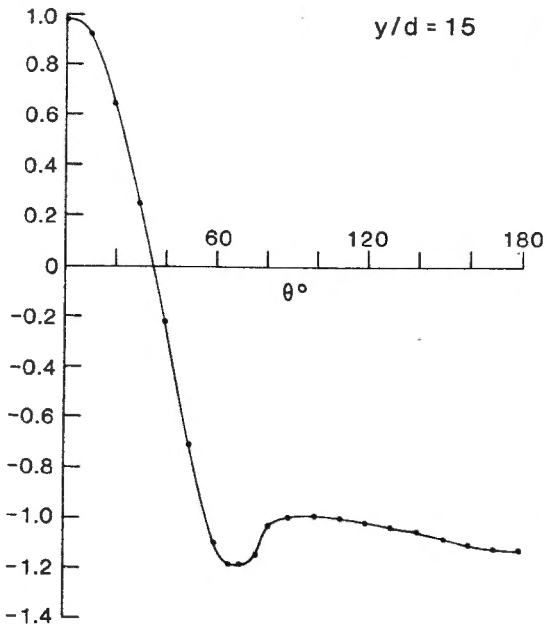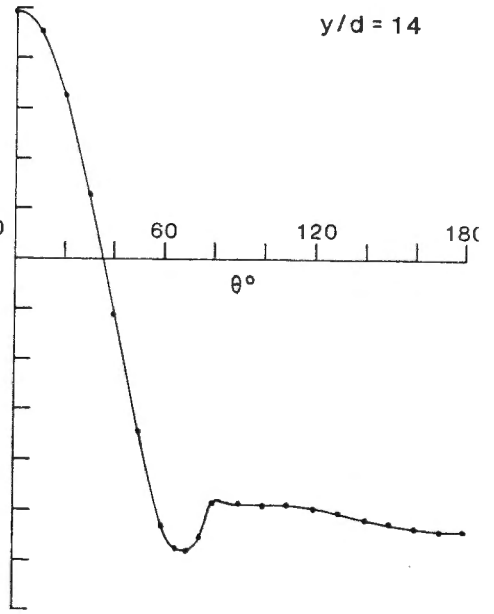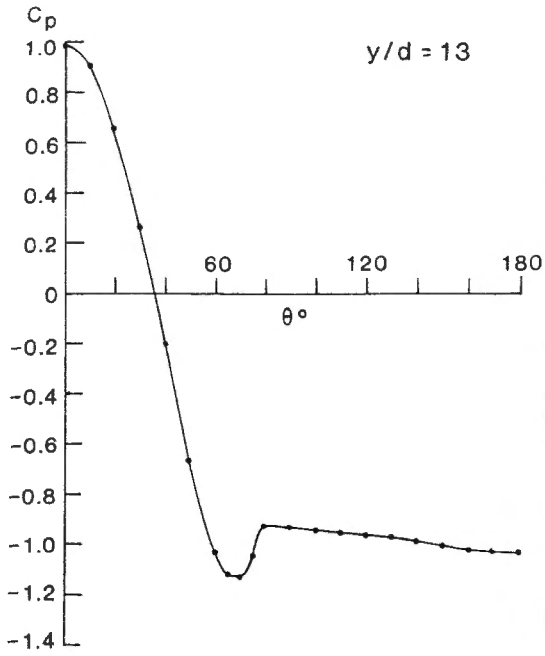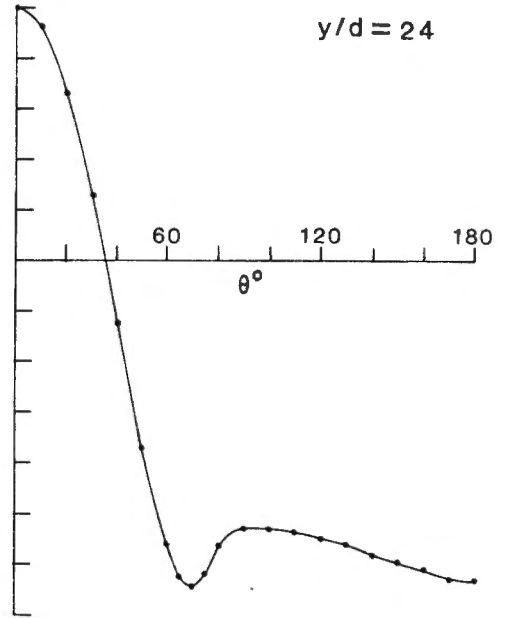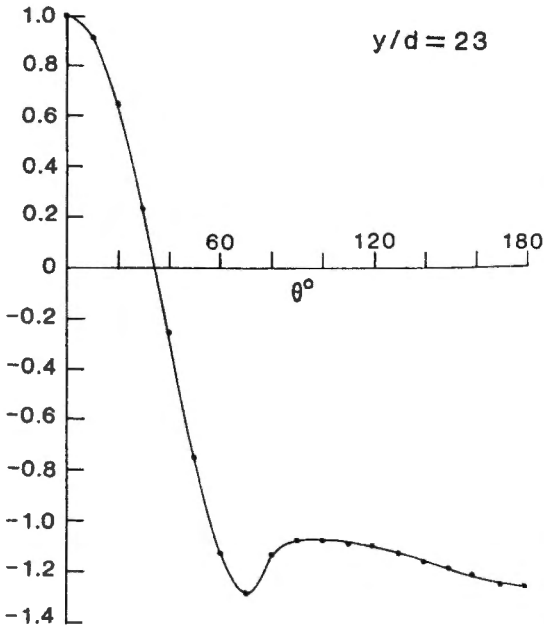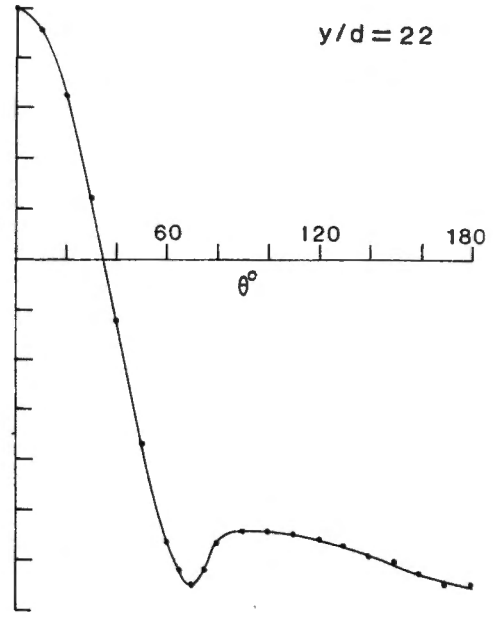
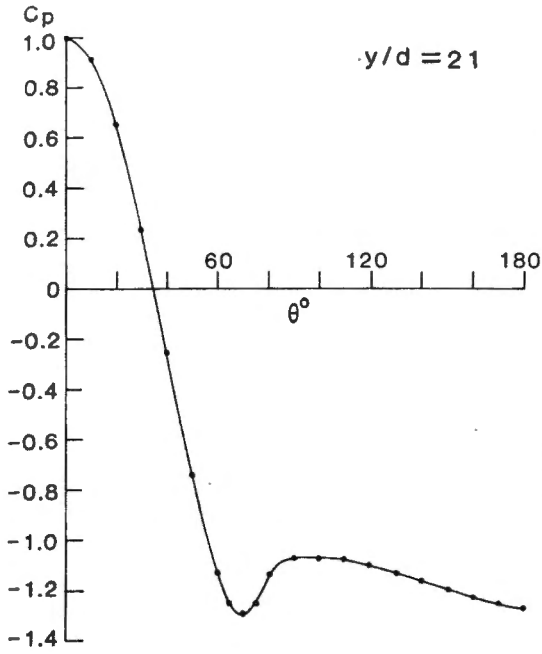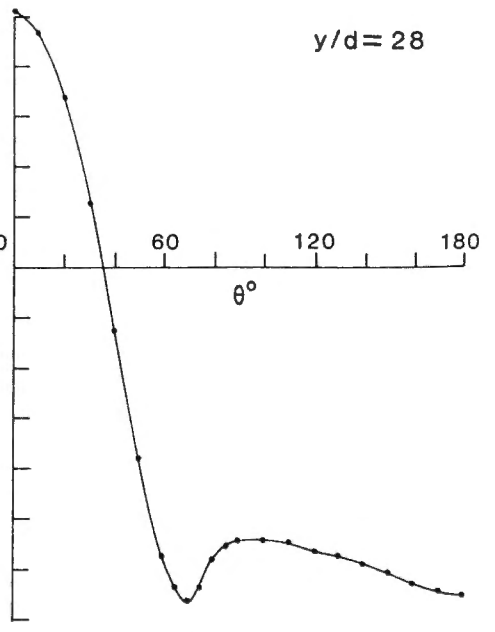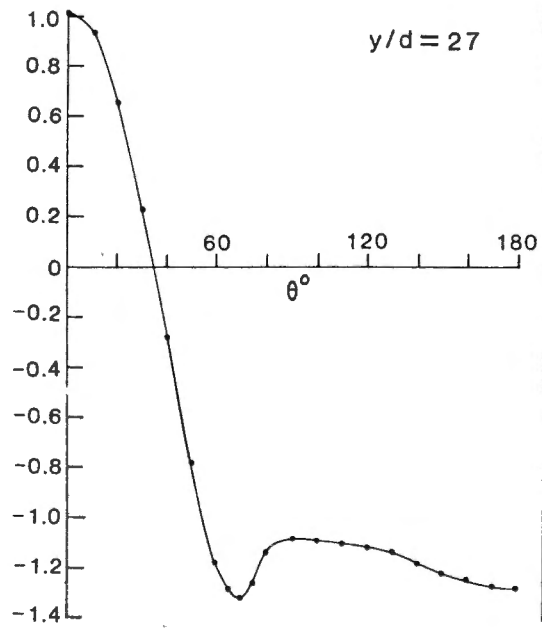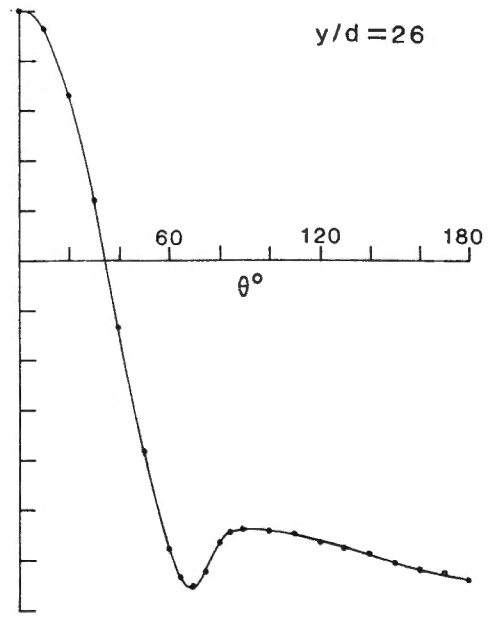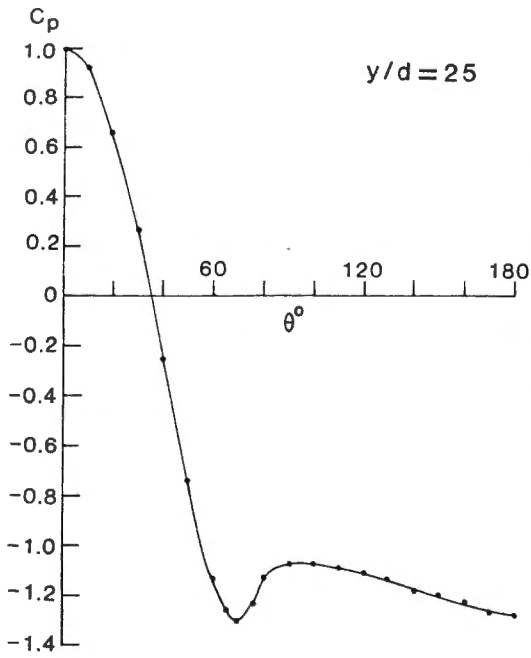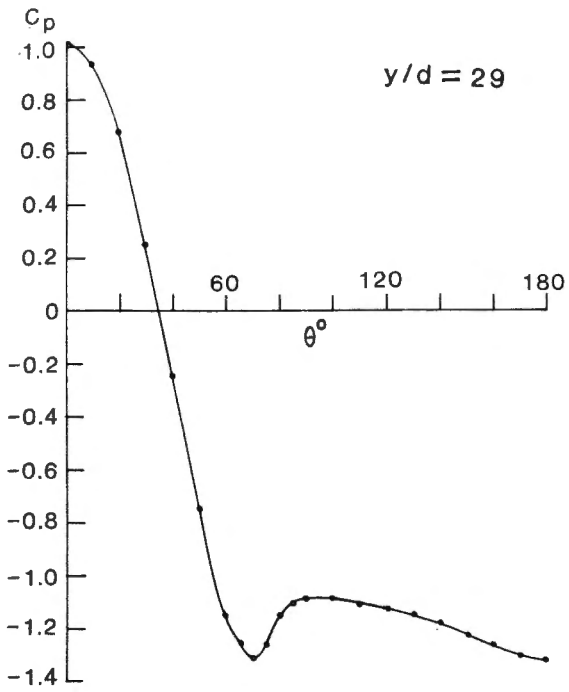| CE No.	TITLE	AUTHOR(S)	DATE
92	Out-of-plane Buckling Formulae for Beam-Columns/Tie-Beams	KITIPORNCHAI S. & WANG C.M.	Oct. 1988
93	An Experimental Investigation of Anchor Bolts under Shear	UEDA T., KITIPORNCHAI S. & LING K.	Oct. 1988
94	New set of Buckling Parameters for Monosymmetric Beam-Columns/Tie-Beams	WANG C.M. & KITIPORNCHAI S.	Nov. 1988
95	Limit Analysis of Welded Tee-end Connections for Hollow Tubes	STEVENS N.J. & KITIPORNCHAI S.	Nov. 1988
96	Flexural-Torsional Buckling of Monosymmetric Beam-Columns/Tie-Beams	KITIPORNCHAI S. & WANG C.M.	Dec. 1988
97	Nonlinear Analysis of Thin-walled Structures Using One Element per Member	AL-BERMANI F.G.A. & KITIPORNCHAI S.	Dec. 1988
98	Co-ordinate Systems for Plastic Yield Surfaces Stress and Strain Space Theories	MEEK J.L. & SU Yinong	Dec. 1988
99	Buckling of Suspended I-beams	DUX P.F. & KITIPORNCHAI S.	Dec. 1988
100	Depth-averaged Equations for Turbulent Free-Surface Flow	PATERSON D.A. & APELT C.J.	Dec. 1988
101	Elasto-plastic Large Deformation Analysis of Thin-walled Structures	AL-BERMANI F.G.A. & KITIPORNCHAI S.	April 1989
102	On the Yield Condition and Optimum Point-wise Reinforcement for Fracturing Continua	BAKER G.	May 1989
103	Brick Walls Spanning Vertically: a Theoretical Investigation of the Capacity to Resist Out-of-plane Wind Loads	MULLINS P. & O'CONNOR C.	June 1989
104	A Uniaxial Model for the Thermo-mechanical Behaviour of Concrete at Elevated Temperatures	KHENNANE A.& BAKER, G.	June 1989
105	Time-dependent Shortening of Reinforced Concrete Columns	McADAM P.S. & BEHAN J.E.	August 1989
106	Simple Vehicle Model for Highway Bridge Impact	CHAN H.T.T. & O'CONNOR C.	Sept. 1989
107	Wheel Loads from Highway Bridge Strains: Field Studies	CHAN H.T.T. & O'CONNOR C.	Sept. 1989
108	Brick Shear Walls: Experimental Investigation of Brickwork-to-Concrete Interface	MULLINS, P & O'CONNOR,C.	July 1990
109 110 111	Measurement of Fluctuating Effects on Circular Cylinder in Uniform Flow at Sub-critical Reynolds Nrs:Parts 1,2,3.	WEST, G.S. & APELT, C.J.	July 1990

CE No.	TITLE	AUTHOR(S)	DATE
112	Shooting-Optimization Technique for Large Deflection Analysis of Structural Members	WANG C.M. & KITIPORNCHAI S.	July 1990
113	Parametric Study on Distortional Buckling of Monosymmetric Beam-Columns	WANG C.M., CHIN C.K. & KITIPORNCHAI S.	July 1990
114	Mathematical Descriptions of the Mechanical Properties of Skeletal Muscle: A Review	GATTO F. & SWANNELL P.	July 1990
115	Buckling of Columns: Allowance for Axial Shortening	WANG C.M., KITIPORNCHAI S. & AL-BERMANI F.G.A.	July 1990
116	Buckling of Restrained Columns with Shear Deformation and Axial Shortening	WANG C.M., XIANG Y. & KITIPORNCHAI S.	July 1990
117	Integrated View of Methods in Buckling Analysis	WANG C.M. & KITIPORNCHAI S.	Aug. 1990
118	On the Use of End Plates with Circular Cylinders in Wind Tunnel Studies	FOX T.A. & WEST G.S.	Aug. 1990
119	Stability of Thin-Walled Members with Arbitrary Flange Shape and Flexible Web	CHIN C.K., AL-BERMANI F.G.A. & KITIPORNCHAI S.	Sept. 1990
120	Single-Equation Yield Surfaces for Monosymmetric and Asymmetric Sections	KITIPORNCHAI S., ZHU K., XIANG Y. & AL-BERMANI F.G.A.	Sept. 1990
121	Nonlinear Analysis of Transmission Towers	AL-BERMANI F.G.A. & KITIPORNCHAI S.	Oct. 1990
122	Formex Formulation of Transmission Towers	AL-BERMANI F.G.A., KITIPORNCHAI S. & CHAN S.L.	Nov. 1990
123	Elasto-plastic Analysis of Space Frames with Flexible Joints	AL-BERMANI F.G.A. & KITIPORNCHAI S.	Nov. 1990
124	Elasto-plastic Large Deflection Analysis of Box Beam-Columns Including Local Buckling Effects	CHAN S.L., KITIPORNCHAI S. & AL-BERMANI F.G.A.	Nov. 1990
125	Column Buckling Under General Loads with Allowances for Shear and Axial Deformations	XIANG Y., WANG C.M. & KITIPORNCHAI S.	Dec. 1990
126	Flow Around 2 Circular Cylinders Arranged Perpendicular to Each Other	FOX T.A.	Dec. 1990
127	A Computerized Data Acquisition System for the Boundary Layer Wind Tunnel	GINGER J.D. & LETCHFORD C.W.	Dec. 1990
128	Wave Set-up, Wave Run-up and Beach Water Table: Interaction Between Surf Zone and Groundwater Hydraulics	GOURLAY M.R.	Dec. 1990
129	Ultimate Strength of Geometrically Imperfect Angle Columns	CHAN S.L. & KITIPORNCHAI S.	April 1991

CIVIL ENGINEERING PUBLICATIONS

(Please add $5 postage & handling to each price)

COASTAL HYDRAULICS & SEDIMENT TRANSPORT IN A COASTAL SYSTEM
by M.R.Gourlay & C.J.Apelt - $16.00

75 YEARS OF CIVIL ENGINEERING AT THE UNIVERSITY OF QUEENSLAND
by M.R.Gourlay and J.L.F.Hacker (1985) - $5 (includes postage)

EARTHMOVING OPERATIONS ANALYSIS WORKSHOP NOTES
by D.G.Carmichael (1985)   - $10.00

PIONEER RIVER ESTUARY - SEDIMENTATION STUDIES
by M.R.Gourlay and J.L.F.Hacker (1986), 207 pages,
98 figures, hard cover. $20.00

SOIL MECHANICS THEORY, COMPUTATION & LABORATORY PRACTICE
Major contributors: Prof. John Atkinson,Assoc.Prof. Ian Donald,
Dr David Potts & Dr John Carter (1987) - $40.00

PILING & RECENT DEVELOPMENTS IN DESIGN & PRACTICE
Major contributors: Assoc.Prof.Mark Randolph, Dr Gary Chapman,
Mr Julian Seidel, Mr David Nolan and Mr Slav Tchepak
- $45.00

APPLICATION OF SOIL MECHANICS THEORY
Major contributors: Prof. Jim Graham, Dr John Carter
& Dr David Williams (1990) - $50.00